The link between volcanism and deglaciation in Iceland

J. Maclennan, M. Jull, D. Mckenzie, L. Slater, K. Grönvold

Geochemistry Geophysics Geosystems G3
AN ELECTRONIC JOURNAL OF THE EARTH SCIENCES
Published by AGU and the Geochemical Society

Article
Volume 3, Number 11
5 November 2002
1062, doi:10.1029/2001GC000282
ISSN: 1525-2027

The link between volcanism and deglaciation in Iceland

J. Maclennan
Bullard Laboratories, Department of Earth Sciences, Madingley Road, Cambridge, CB3 0EZ, UK

Now at Laboratoire de Geosciences Marines, Institut de Physique du Globe de Paris, 4, Place Jussieu, 75005 Paris, France. (maclenna@ipgp.jussieu.fr)

M. Jull
Bullard Laboratories, Department of Earth Sciences, Madingley Road, Cambridge, CB3 0EZ, UK

Now at Department of Geology and Geophysics, Woods Hole Oceanographic Institution, Woods Hole, Massachusetts 02543, USA. (mjull@whoi.edu)

D. McKenzie
Bullard Laboratories, Department of Earth Sciences, Madingley Road, Cambridge, CB3 0EZ, UK (mckenzie@esc.cam.ac.uk)

L. Slater
Bullard Laboratories, Department of Earth Sciences, Madingley Road, Cambridge, CB3 0EZ, UK

Now at Amerada Hess Limited, 33 Grosvenor Place, London, UK. (l.slater@amhess.co.uk)

K. Grönvold
Nordic Volcanological Institute, Reykjavik, Iceland (karl@norvol.his.is)

[1] Temporal variation in the eruption rate and lava composition in the rift zones of Iceland is associated with deglaciation. Average eruption rates after the end of the last glacial period, ~12 kyr BP, were up to 100 times higher than those from both the glacial period and recent times (<5 kyr BP). This peak in volcanic activity finished less than 2 kyr after the end of deglaciation. New geochemical data from ~80 basalt and picrite samples from the Theistareykir and Krafla volcanic systems show that there is a temporal variation in both the major and trace element composition of the eruptions. Early postglacial eruptions show a greater range in MgO contents than eruptions from other times, and at a fixed MgO content, the concentration of incompatible elements in subglacial eruptions is higher than that in early postglacial eruptions. Recent eruptions from the Krafla system have similar compositions to subglacial eruptions. The high eruption rates and low rare earth element (REE) concentrations in the lava from early postglacial times can be accounted for by increased melt generation rates in the shallow mantle caused by unloading of an ice sheet. Magma chamber processes such as crystallization and assimilation can produce the temporal variation in REE contents if garnet is present. However, garnet is not observed as a phenocryst or xenocryst phase and is not required to match the variation in major element contents observed at Krafla and Theistareykir. If the increase in eruption rates reflects increased melt production rates in the mantle, then the relative timing of deglaciation and the burst in eruption rates can be used to estimate the rate of melt transport in the mantle. The observed duration of enhanced eruption rates after deglaciation can be reproduced if the vertical melt extraction velocity is >50 m yr^{-1}.

Components: 13,064 words, 11 figures, 2 tables.

Keywords: Iceland; glaciation; mantle melting; magma migration; magma chambers; igneous rocks.

Index Terms: 3035 Marine Geology and Geophysics: Midocean ridge processes; 3640 Mineralogy and Petrology: Igneous petrology; 8434 Volcanology: Magma migration; 1223 Geodesy and Gravity: Ocean/Earth/atmosphere interactions (3339).

Received 27 November 2001; **Revised** 10 April 2002; **Accepted** 10 April 2002; **Published** 5 November 2002.

Maclennan, J., M. Jull, D. McKenzie, L. Slater, and K. Grönvold, The link between volcanism and deglaciation in Iceland, *Geochem. Geophys. Geosyst.*, *3*(11), 1062, doi:10.1029/2001GC000282, 2002.

1. Introduction

[2] Iceland is an excellent place to study the influence of glaciation on volcanic activity because it has been extensively glaciated throughout Pleistocene times [*Sæmundsson*, 1980]. The climate record from the Greenland ice cores shows that the last major glaciation of the North Atlantic region (the Weichselian period) started ~70 kyr BP (before present) and ended ~12 kyr BP [*Mayewski and Bender*, 1995]. There is widespread volcanic activity on Iceland because it is situated where a hot upwelling mantle plume lies beneath the Mid-Atlantic Ridge. This upwelling generates the melt that crystallizes to form the thick Icelandic crust. The bulk of the plate divergence occurs in active rift zones, which host many young basaltic eruptions. This glaciation of a spreading ridge provides a unique opportunity to study the effect of rapid unloading on magmatic processes at ridges, and observations from Iceland can provide constraints on geochemical and physical models of the generation, transport, and crystallization of magma.

[3] The link between deglaciation and increased volcanic activity has been noted in several different parts of the neovolcanic zones of Iceland (Figure 1); on the Reykjanes Peninsula of southwest Iceland [*Jakobsson et al.*, 1978], in the Veidivötn fissure swarm of southern Iceland [*Vilmundardóttir and Larsen*, 1986], at the Dyngjufjöll region of central Iceland [*Sigvaldason et al.*, 1992], and at the Theistareykir volcanic system in the north of Iceland [*Slater et al.*, 1998]. Two models have been proposed to link ice unloading with an increase in eruption rates. In the first, the change in the state of stress of the crust caused by the removal of the ice sheet allows increased tapping of magma chambers and increased eruption rates [*Gudmundsson*, 1986]. In contrast, *Jull and McKenzie* [1996] modelled the effect of ice unloading on mantle melting and found that decompression during deglaciation can produce a large increase in mantle melting rates, which may in turn be reflected by an increase in eruption rates. It is important to note that the *Jull and McKenzie* [1996] models only apply to melt generation in parts of the rift system where the mantle upwelling is thought to be controlled by passive plate separation alone. Therefore their models are not applicable to areas close to the plume center where active upwelling may be important, such as Dyngjufjöll and the Eastern Volcanic Zone [*Maclennan et al.*, 2001b; *Ito et al.*, 1999].

[4] Three studies have documented variation in the geochemistry of the eruptives that occurs at the time of deglaciation; at the alkaline Sænfellsnes volcano in western Iceland [*Hardarson and Fitton*, 1991], the Theistareykir volcanic system [*Slater et al.*, 1998] and the Reykjanes Peninsula [*Gee et al.*, 1998a]. The observations at Sænfellsnes were attributed to changes in mantle melting conditions resulting from decompression at the time of deglaciation by *Hardarson and Fitton* [1991]. Unfortunately the cause of melting away from the ridge axis at flank zones like Sænfellsnes remains poorly understood, and this limits the usefulness of comparison of observations and melting model results in this case. The mantle decompression models of *Jull and McKenzie* [1996] predict that melts generated during unloading should have different rare earth element (REE) concentrations to melts produced at other times and *Slater et al.* [1998] demonstrated that these decompression models can match the observed change in geochemistry between the largest glacial and postglacial eruptions in the Theistareykir volcanic system. However, *Gee et al.* [1998a] proposed that the geochemical variations observed on the Reykjanes Peninsula and at Theistareykir may be caused by processes that occur in crustal

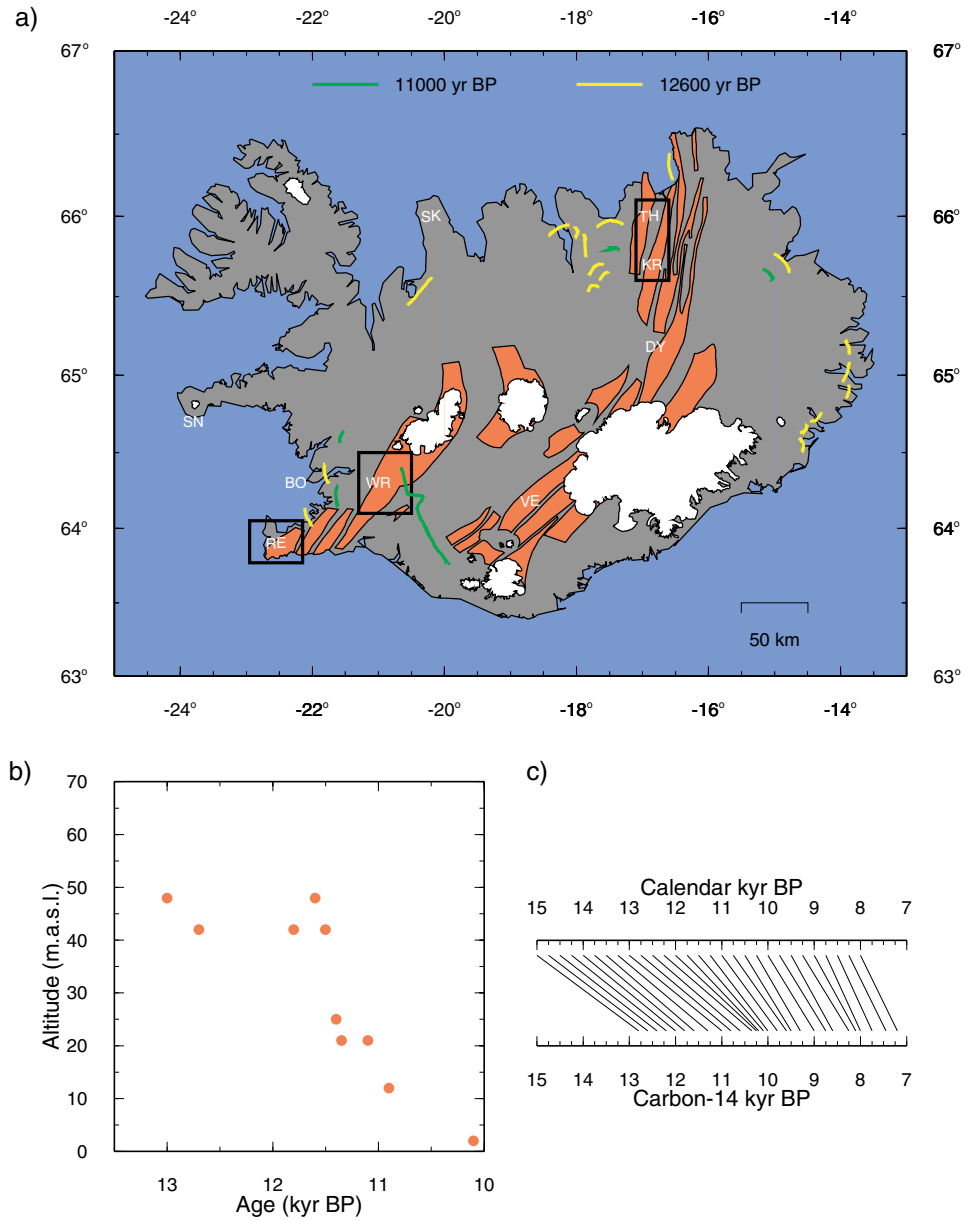

Figure 1. (a) Summary map of Iceland, after *Einarsson and Sæmundsson* [1987]. Active fissure swarms are shown in orange and lie where plate divergence is taking place. Thick lines show the location of terminal moraine complexes redrawn from *Ingólfsson et al.* [1997], and the ages of the complexes are shown at top of map. Dashed lines enclose study areas. Letters show locations mentioned in the text: BO, Borgarfjordur; SK, Skagi Peninsula; SN, Snaefellsnes Peninsula; DY, Dyngjufjöll; VE, Veidivötn fissure swarm; RE, Reykjanes Peninsula; WR, Western Rift Zone; KR, Krafla; TH, Theistareykir. (b) Relative sea level curve from the Skagi Peninsula after *Rundgren et al.* [1997]. The measurements are given in meters above present day sea level. (c) Conversion from ^{14}C yr BP to calendar m yr BP, after *Stuiver and Reimer* [1993].

magma chambers such as crystallization, assimilation, and mixing. They argued that the distinctive composition of early postglacial magmas was caused by reduced residence times in the crust at the time of glacial unloading and isostatic rebound. However, these workers did not attempt to quantify the observed geochemical variations in terms of magma chamber processes. Furthermore, they did not present physical arguments to show that unloading of the ice sheet could occur without influencing melting of the mantle. The expected response of the stress state of the Earth to glacial

unloading and the melt generation by decompression under mid-ocean ridges is summarized by *Jull and McKenzie* [1996], and the simple physical arguments that they present show that it is extremely difficult to prevent an increase in melt production rates at the time of deglaciation, regardless of the nature of the magmatic processes in the overlying crust.

[5] Therefore although it is widely accepted that glacial unloading influences both the eruption rates and composition of Icelandic basalt, the significance of this influence is not yet clear. If magma chamber processes alone control the response of the magmatic system to unloading, the variation in eruption rate and lava composition potentially provides constraints on models of melt bodies in the Icelandic crust. Alternatively, if mantle melting controls this response, the geochemical variation and timing of the change in eruption rates can be used to estimate the melt fraction against depth relationship and the rate of melt extraction from the mantle [*Slater et al.*, 1998].

[6] The purpose of this work is to evaluate the circumstances under which either mantle melting or magma chamber processes can produce the observed temporal variation in lava composition. New analyses of the major and trace element compositions of 80 samples from the Theistareykir and Krafla volcanic systems are presented. The results of geochemical models of mantle melting and magma chamber processes are compared with the Krafla and Theistareykir data in section 5. Estimates of eruption rates from four parts of the rift zones are given in section 3, and the relative timing of the deglaciation and the burst in eruption rates is later used to constrain the vertical melt velocity under the rift zones of Iceland.

2. Glacial History

[7] Quantifying the timing of major changes in ice sheet size and eruption rate forms a vital part of our understanding of the link between deglaciation and volcanism. The last major deglaciation of Iceland took place between 15 and 10 kyr BP when the ice sheet retreated from outside the present coast line to roughly its present size. When modelling the effects of ice unloading on magmatic processes, it is important that constraints be placed on details such as the rate of ice removal and the number of phases of advance and retreat during the transition from glacial to postglacial conditions. Unfortunately, it is not possible to make a complete reconstruction of the deglaciation since many of the morphological features that could have been used to delimit the ice-load dimensions through time have been removed by erosion. Nonetheless, several workers have been able to make age estimates of moraine complexes using carbon-14 dates from organic material found in sediments related to the moraine. The uncertainty in the ^{14}C dates is typically ~100 years. All ages presented in this paper are in calendar years before present, and ^{14}C ages have been converted using the scheme of *Stuiver and Reimer* [1993] (Figure 1). Some of the oldest moraine associated with the last deglaciation is found in Borgarfjordur, SW Iceland, where the ice sheet stood within 10 km of the present-day coast around 14,000 yr BP [*Ingólfsson et al.*, 1997]. Basal dates of ~14,000 yr BP from sediment cores taken on the Iceland Shelf indicate that much of the inner shelf may have been ice-free at this time [*Andrews et al.*, 2000; *Jennings et al.*, 2000]. Two events at ~12,600 yr BP and 11,000 yr BP formed end-moraine complexes which can be traced around much of Iceland (see Figure 1a and review by *Ingólfsson and Norddahl* [1994]). The older set of moraines was created by a glacier with a radius of ~180 km, while the younger set lies ~20 km further inland. The results of detailed study of moraine complexes and lacustrine sediments from South Iceland are consistent with a deglaciation model in which the ice margin lay more than 25 km inside the present day coastline between 12,600 yr BP and 11,000 yr BP [*Geirsdóttir et al.*, 2000].

[8] The relative sea level history of Icelandic coastal areas provides a means of constraining the ice sheet dimensions between times of moraine formation. When the ice load depresses the land surface, relative sea levels are high, and when the ice is removed, rebound takes place rapidly due to the relatively low viscosity of the upper mantle underlying Iceland. Viscosity estimates for the Icelandic

mantle lie in the range 10^{18}–10^{19} Pa s, and these correspond to a characteristic rebound time of 100–1000 yr for a glacier with a radius of ~200 km [*Sigmundsson and Einarsson*, 1992]. Dating of raised beaches and marine deposits found inside the present coastline has been used to investigate relative sea level changes. About 14,500 yr BP sea level at Borgarfjordur was more than 60 m above present sea level in response to an extensive ice-sheet [*Ingólfsson et al.*, 1997]. Although the ice margin moved an unknown distance inland between ~14,000 yr BP and the formation of the ~12,600 yr BP moraines, there is no record of relative sea levels falling below 40 m. Since relative sea levels ~11,000 yr BP also stood at 40 m, it is unlikely that the glacier retreated further than the position of the ~11,000 yr BP moraines between 14,000 yr BP and 12,600 yr BP. The relative sea level curve between 13,000 yr BP and 10,000 yr BP is well recorded on the Skagi Peninsula in northern Iceland; as rebound took place, a series of lakes now at different altitudes became isolated from marine influence at different times [*Rundgren et al.*, 1997]. Figure 1 shows that relative sea level remained high between ~13,000 yr BP and ~11,800 yr BP and then dropped rapidly by ~50 m in under 1000 years. The relative sea level reconstruction for the Reykjavik area made by *Ingólfsson et al.* [1995] also shows rapid rebound starting ~11,800 yr BP and lasting ~1 kyr. By ~10,200 yr BP, coastal rebound was complete, and the presence of ash bands and subaerial eruptions in south/central Iceland suggests that the ice sheet had almost reached its present size [*Sæmundsson*, 1992]. The maximum height of the glacier during the last glacial period is not known, but the elevation of table mountains which erupted through the ice sheet is up to 1 km above the surrounding plain, so the ice was at least 1 km thick in places. Although the relationship between Icelandic and North Atlantic climate and ice sheet dimensions is not yet fully understood, it is likely that the retreat of the ice was related to a rapid warming event between 11,800 yr BP and 10,300 yr BP that has been inferred from biostratigraphic records [*Rundgren*, 1995]. In summary, although the ice sheet margins lay inside the present coast from 14,500 yr BP onward and there were several small advances and retreats after that time, the final deglaciation of Iceland was dominated by a rapid unloading event between ~11,800 and ~10,300 yr BP.

3. Volcanic Record

[9] It is important to determine the age and volume of eruptions in order to characterize the early postglacial burst in volcanic activity. Eruptions from the last glaciation and postglacial times can be given relative ages using morphology and tephrochronology. Large subglacial eruptions are often preserved as table mountains which have steep sides of pillow lava and hyaloclastite and are capped by subaerial flows where the eruption broke through the ice surface. Another common subglacial eruptive morphology is the hyaloclastite ridge. Subaerial eruptions form relatively shallow-sloping lava shields or flows from fissures, with surface features such as pahoehoe, a′a, tumuli, and hornitos. If subaerial flows are glaciated, the surface features are eroded off and covered with glacial deposits, allowing the distinction to be made between flows from postglacial times and those from previous interglacials. Postglacial eruptions can be dated using tephrochronology, and bounds on the absolute ages of flows can be provided by dating of organic material found associated with the ash layers which lie stratigraphically above and below the eruption.

[10] The volume of eruptions was estimated using geological and topographical maps. Figure 2 shows the outcrop of early postglacial lava in the four study areas. At Theistareykir and the Western Rift Zone the exposed area of early postglacial eruptions (12–7 kyr BP) is much greater than that of younger flows, despite the covering of older flows by younger flows. The outcrop area of early postglacial flows is similar to that of younger flows at both Reykjanes and Krafla. Many eruptions during early postglacial times formed lava shields which consist of thick sequences of compound lava flows in the shield apron and cones which have a height 10s to 100s of meters above the base of the lava shield [*Rossi*, 1996]. In contrast, volcanic activity in the last 7 kyr has been dominated by eruptions from fissures which produce relatively thin flows, typically less than 10 m in thickness. There are

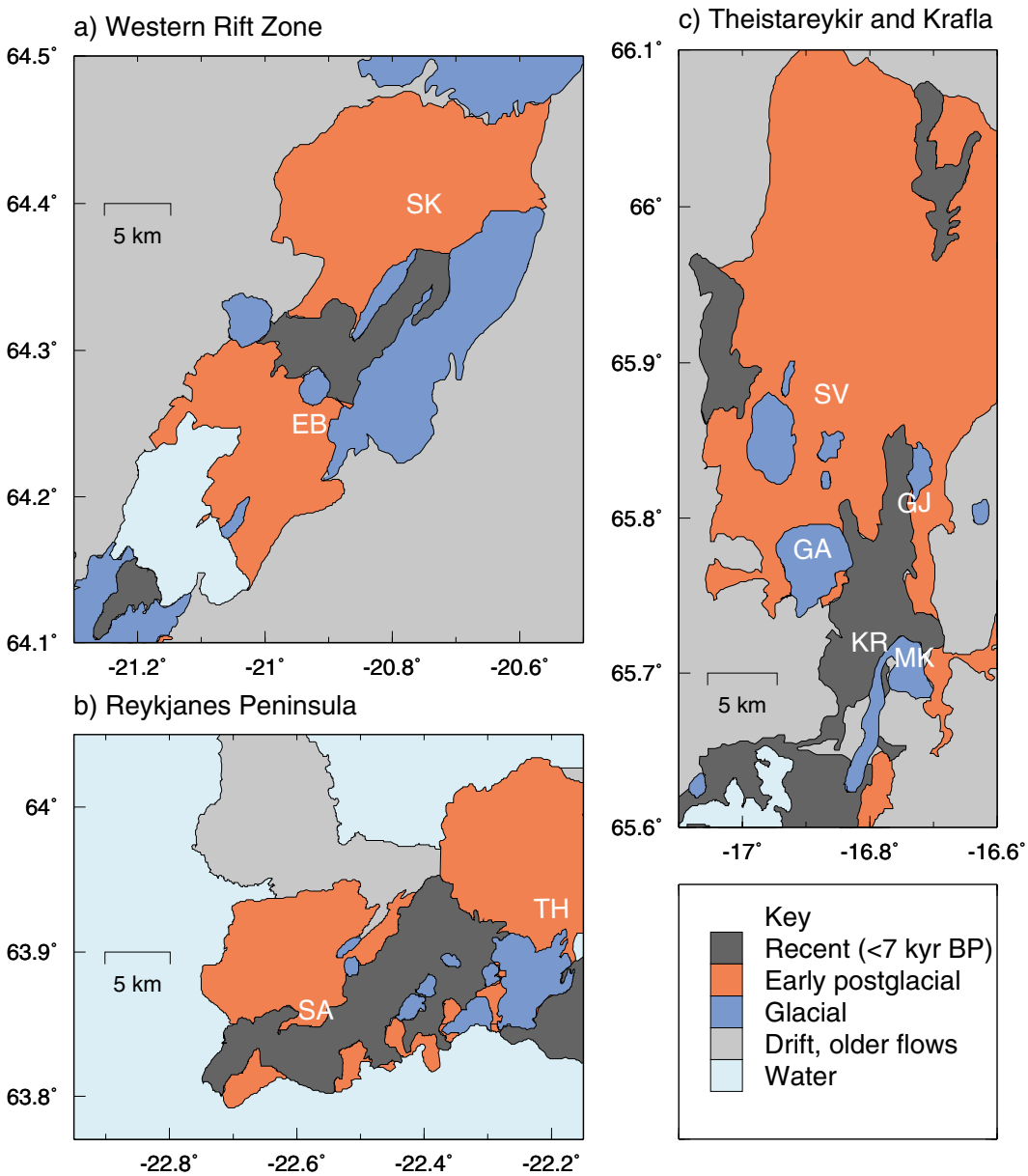

Figure 2. Maps of volcanic zones showing approximate outcrop area of subglacial, early postglacial and recent eruptions, based on maps of *Sæmundsson* [1991, 1992, 1995] and *Jakobsson et al.* [1978]. The approximate source location for large eruptions mentioned in the text are also shown.(a) Western Rift Zone: SK, Skjaldbreidur; EB, Eldborgir. (b) Reykjanes Peninsula: TH, Thrainnskjoldur; SA, Sandfellshaed. (c) Krafla and Theistareykir: SV, Stóravíti; GA, Gæsafjöll; GJ, Gjástykkisbunga; MT, Krafla Mountain subglacial eruption; KR, 1975–1984 Krafla fissure eruptions.

errors in volume estimates of eruptions caused by erosion and burial of volcanoes and uncertainty in flow thicknesses. These errors are most severe for glacial eruptions, which may have been subject to extensive erosion and burial. Therefore the volume and eruption rate estimates for glacial times are minimum bounds. However, it is easy to identify the few flows that dominate the postglacial volumetric output in most of the active volcanic zones of Iceland.

[11] It is possible to reconstruct the eruption rates through time for the areas shown in Figure 2, and the details of the reconstruction method are given using the Theistareykir system as an example. For each eruption a volume is estimated, along with upper and

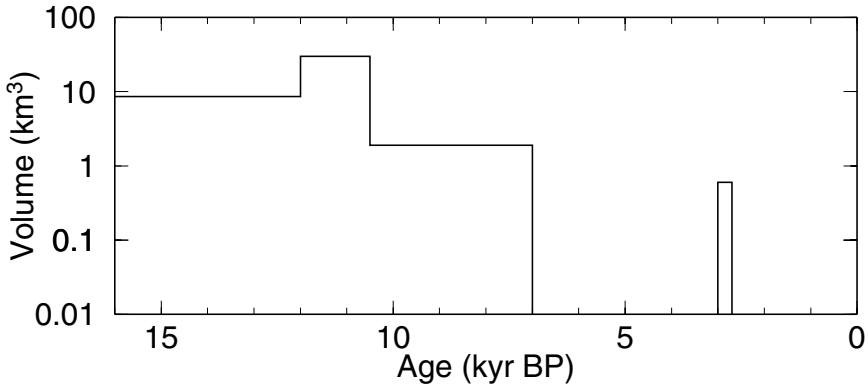

Figure 3. Summed volumes of Theistareykir eruptions plotted against age. The value is obtained by summing the volumes of all eruptions whose ages lie between the age bounds. The glacial age bounds are at 70,000 and 12,500 yr BP, and the other age bounds used for Theistareykir are at 10500, 7000, 3000, and 2700 yr BP.

lower age bounds. For example, the lava shield Stóravíti has a volume of ~30 km^3, is postglacial (younger than 12 kyr BP), and underlies an ash band that was deposited ~10.5 kyr BP. Between each age bound, the volumes were summed as shown in Figure 3. This sum shows that the total volume erupted between 12 kyr BP and 10.5 kyr BP is over 10 times greater than the total volume erupted between 10.5 kyr BP and the present day. Then the summed volumes between each age bound were divided by the length of time between the bounds to give an average eruption rate in $km^3\ kyr^{-1}$, so the eruption rate between 12 kyr BP and 10.5 kyr BP is given by the summed volume of 30.3 km^3 divided by 1.5 kyr. The eruption rates are summarized in Table 1. Figure 4 shows this eruption rate normalized in two different ways so that it is possible to compare eruption rates between areas of different size. The rate in $km^3\ kyr^{-1}$ was divided by the total erupted volume of the area in the last 74 kyr to give a rate in $\%\ kyr^{-1}$ (left-hand axis) and by the along-axis length of the area to give $km^2\ kyr^{-1}$ (right-hand axis). Also shown on Figure 4 is an estimate of the maximum bound on mean eruption rate using a 1000 year running window. This maximum bound was calculated by using the age constraints on the eruptions to find the total volume of material that could have been erupted within a given 1000 year window. Then this volume was divided by 1000 years to give an eruption rate.

[12] In each area the eruption rates immediately after deglaciation were 30–50 times higher than those from more recent times and the minimum estimates from glacial times. These high eruption rates persisted for <1.5 kyr after the deglaciation of each area. During this time interval (15% of the postglacial period) more than 75% of the total postglacial volume was erupted. The maximum bound on mean eruption rates plotted on Figure 4 demonstrates that the peak in eruption rates is not an artifact caused by variation in time intervals between the bounding ash bands, and eruption rates during the early postglacial peak are ~20 times higher than those from any 1000 year interval during more recent times. Unfortunately, variations in eruption rate during the glacial period cannot be resolved due to the large uncertainties in both age and volume of glacial eruptions. The most important geological observations used to produce the reconstructions are outlined below.

3.1. Theistareykir and Krafla

[13] About 70% of the volume of preserved eruptives from the Theistareykir system that are younger than 74 kyr is contained in the lava shield Stóravíti (~30 km^3). Since Stóravíti retains its surface fea-

Table 1. Average Eruption Rates in Study Areas ($km^3\ kyr^{-1}$)[a]

Location	Age Range, kyr BP		
	Glacial 74.0–12.5	Early Postglacial 12.5–10.0	Recent 10.0–0.0
Theistareykir	0.13	12.12	0.26
Krafla	0.03	1.32	0.03
Western Rift Zone	0.50	11.25	0.34
Reykjanes	0.05	3.76	0.15

[a] Estimates for glacial period are a lower bound.

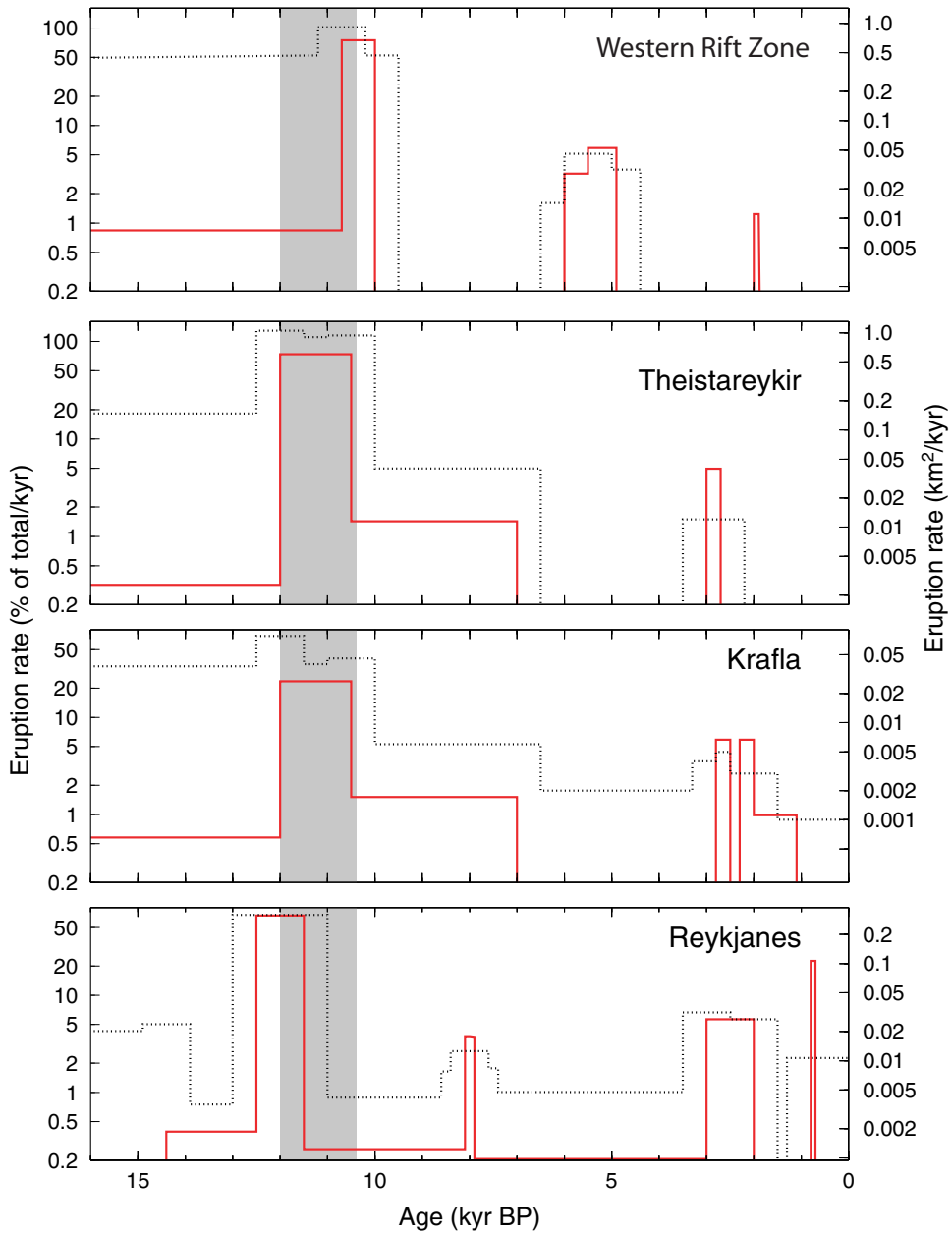

Figure 4. Reconstruction of eruption rates through time for four study areas. Note that the vertical axis is a log scale. For each area, the left-hand axis shows the proportion of total erupted volume in last 74 kyr produced per kyr. The right hand axis shows the eruption rate normalized by the length of the study area parallel to the ridge. The shaded area on each plot shows the time of postglacial rebound. The red line shows the average eruption rate and the dotted line shows the maximum bound on the eruption rate, both calculated as described in the text.

tures over almost all of its area, it postdates the deglaciation of the Theistareykir area. Stóravíti is younger than the Vedde ash layer (~12,000 yr BP [*Sæmundsson*, 1991; *Grönvold et al.*, 1995]), but older than an ash layer known as the S layer. The S layer is thought to have been deposited ~10,500 yr BP, judging by the sediment thickness between it and the Saksunarvatn ash (~10,200 yr BP [*Grönvold et al.*, 1995; *Björck et al.*, 1992]). Hence, Stóravíti was erupted before the completion of isostatic rebound. The largest preserved subglacial eruption at Theistareykir is the table mountain Gæsafjöll, which has a volume of ~5 km^3 at the present day. Although the eruption rates at Krafla are much lower than those at Theistareykir, the timing of the burst is similar. The largest postglacial

eruption is the lava shield Gjástykkisbunga, which has a volume of ~2 km^3 and is of similar age to Stóravíti [*Sæmundsson*, 1991].

3.2. Western Rift Zone

[14] According to the maps of *Sæmundsson* [1992], the postglacial eruptive budget of the Western Rift Zone is dominated by two early postglacial lava shields, Skjaldbreidur (17 km^3) and Eldborgir (11 km^3). Since both of these lava shields retain their surface morphological features and lie on land that was on the ice-bound side of a set of moraines formed ~10,800 yr BP, they must be younger than this date. The Eldborgir lava has charred plant remains beneath it which have been dated to ~10,200 yr BP. Field relationships show that Skjaldbreidur is older than Eldborgir, so the peak in postglacial volcanic activity in the Western Rift Zone took place between ~10,800 and 10,200 yr BP.

3.3. Reykjanes Peninsula

[15] Much of the Reykjanes Peninsula has been ice free since ~14,500 yr BP, several thousand years before Krafla, Theistareykir, or the Western Rift Zone underwent deglaciation. *Jakobsson et al.* [1978] made volume estimates of the postglacial eruptions in the area, and *Sæmundsson* [1995] used tephrochronology to date the flows. Between 14,500 and 12,500 yr BP, there were several small picritic eruptions, followed by the production of the lava shields Thrainnskjoldur (4.6 km^3) and Sandfellshaed (4.2 km^3) ~12,500 yr BP. From ~11,500 yr BP to the present day, most eruptions have been small volume fissure flows. Eruption rates increased by a factor of 100 between the period following local deglaciation of the Reykjanes peninsula (14,500–12,500 yr BP) and that which coincides with the final deglaciation of the rest of Iceland (12,500–11,500 yr BP). After the deglaciation had terminated, eruption rates returned to low values.

4. Geochemical Observations

4.1. Sample Acquisition and Analytical Methods

[16] Major, trace element and REE concentrations were obtained for ~250 samples from the Theistareykir and Krafla volcanic systems. The data for Theistareykir come from *Slater* [1996] and while some of the analyses have been published by *Slater et al.* [1998] and *Slater et al.* [2001], the analyses for 30 subglacial samples are presented here for the first time. The Krafla samples were collected by *Nicholson* [1990], and selected major and trace element analyses of the samples were given by *Nicholson et al.* [1991] and *Nicholson and Latin* [1992]. New REE data for 50 Krafla samples are presented here and are shown with the Theistareykir data in Table 2. Major and selected trace element concentrations for both the Theistareykir and the Krafla sample sets were analyzed by X-ray fluorescence at the University of Edinburgh using the technique described by *Fitton et al.* [1998]. For REE analysis, the samples were prepared by dissolution in HF and then REE concentrations were measured on the research ICP-MS at the NERC facility at Silwood Park using the method described by *Slater* [1996] and *Maclennan et al.* [2001b]. The analytical details are described in greater detail in appendix A. Mean and standard deviations of repeat runs of U.S. Geological Survey standards BHVO-1 and BIR-1 are also given in Table 2. Accuracy and precision is better than ~10% for the REEs and better than 5% for other trace elements such as Sr, Zr, Y, and Sc.

4.2. Composition of Largest Eruptions

[17] Figure 5 shows the normalized REE concentrations for the two largest preserved eruptions in the Theistareykir system; the postglacial lava shield Stóravíti and the subglacial table mountain Gæsafjöll. The composition of Stóravíti is likely to be similar to that of the average lava erupted in Theistareykir during postglacial times, and the composition of Gæsafjöll is the best available estimate of the average composition of subglacial Theistareykir eruptions. The mean Mg # of the Stóravíti samples is 61.6 and that of the Gæsafjöll samples is 59.0. These Mg # values are slightly lower than those expected for primary melts of the mantle and indicate that Stóravíti and Gæsafjöll magmas have experienced modest amounts of fractional crystallization. As noted by *Slater et al.* [1998], the REE contents of Gæsafjöll are higher than those of Stóravíti. While the La content of Gæsafjöll is 3.1 times higher than that of Stóravíti,

Table 2. (Representative Sample) Compositions of Whole-Rock Samples Rrom the Theistareykir and Krafla Volcanic Systems: Majors in wt % Oxide, Traces in ppm [The full Table 2 is available in ASCII tab-delimited format at http://www.g-cubed.org.]

	Theistareykir Samples Sample and eruption names from *Slater* [1996]												
Eruption	Einbui			Kviholafjoll				Baejarfjall		Eilifur	Ketilfjall	Raudholl	
[a]Volume (km^3)	0.100			sv				1.000		sv	sv	sv	
[c]period	g			g				g		g	g	g	
[d]start bound (yr BP)	70000			70000				70000		70000	70000	70000	
end bound	12000			12000				12000		12000	12000	12000	
Sample	9301	9302	9303	9315	9316	9317	9318	9319	9320	9343	9350	9351	9351A
SiO_2	50.26	49.73	50.16	49.34	48.70	48.27	48.54	48.74	48.52	48.72	49.39	48.56	49.37
Al_2O_3	16.10	16.26	15.79	15.29	14.89	14.92	15.01	14.86	15.68	16.04	15.63	14.53	14.81
$Fe_2O_3{}^t$	10.90	10.43	10.96	12.19	12.22	12.05	12.18	13.03	12.04	11.24	13.46	14.30	14.30
MgO	9.41	9.62	8.98	9.67	9.75	9.77	9.92	7.97	8.74	7.36	5.88	6.13	6.10
CaO	12.03	12.22	12.32	11.50	11.44	11.53	11.37	11.71	11.65	12.62	11.43	10.79	10.78
Na_2O	1.93	1.92	1.87	2.03	1.96	1.90	1.93	2.18	2.02	2.05	2.24	2.50	2.56
K_2O	0.14	0.12	0.14	0.20	0.20	0.18	0.20	0.26	0.22	0.27	0.14	0.26	0.27
TiO_2	0.77	0.71	0.80	1.23	1.23	1.32	1.25	1.70	1.46	1.48	1.63	1.99	1.99
MnO	0.18	0.17	0.18	0.19	0.19	0.19	0.19	0.20	0.19	0.18	0.21	0.22	0.23
P_2O_5	0.07	0.07	0.07	0.12	0.12	0.14	0.13	0.18	0.16	0.16	0.18	0.19	0.20
Sc	43.0	39.1	49.8	39.9	41.5	41.3	43.8	45.0	42.9	41.7	50.3	48.4	45.0
V	253.1	242.9	266.1	297.1	294.0	279.3	282.1	320.9	293.0	298.4	366.8	392.2	386.7
Cr	99.9	99.0	110.1	415.5	425.0	471.4	437.7	322.9	311.3	228.7	76.5	44.2	43.4
Co	58.0	53.1	49.8	52.2	57.1	50.3	50.8	53.5	51.8	41.4	39.8	45.2	45.4
Ni	121.2	124.5	102.0	166.5	172.7	183.8	185.6	114.0	149.5	86.7	51.4	46.4	46.9
Cu	122.2	119.2	102.5	92.2	110.3	101.2	92.1	119.7	93.1	113.0	116.5	115.0	119.4
Zn	72.5	66.7	72.5	88.0	87.8	88.3	88.6	99.0	89.0	81.1	105.8	119.4	118.6
Ga	18.2	16.3	17.0	16.6	19.1	18.5	17.7	20.4	20.6	18.6	17.8	21.6	20.4
Rb	3.1	2.9	3.5	3.7	4.4	3.8	4.1	5.2	4.8	5.8	1.5	5.0	5.0
Sr	134.1	133.2	135.3	148.8	148.4	153.7	150.2	174.8	176.6	194.0	145.3	186.0	186.1
Y	15.9	14.5	15.9	21.9	21.8	22.7	21.0	27.7	23.9	22.7	33.0	34.9	34.6

[a] Eruption volume estimates. Small volumes are marked sv.
[b] Summed eruption volume of all recent eruptions.
[c] g - glacial; p - early postglacial; r - recent.
[d] Start bound is the oldest possible age of the eruption, and end bound is the youngest possible age (in years BP).
[e] given in vol%.
[f] Code for names of people who collected the samples or performed the analyses: S, Slater; G, Gronvold; H, Habekost; E, Elliott; N, Nicholson; M, Maclennan.
[g] First line gives method used for analyses. Second line gives code for analyst.
[h] Trace elements excluding REEs, Co, Ga.
[i] Codes for papers where data has already been published: S98 - *Slater et al.* [1998]; S01 - *Slater et al.* [2001]; N92 - *Nicholson and Latin*, [1992]; E91 - *Elliott et al.*, [1991]; O76 O'Nions et al, 1976.
[j] BTHO is a standard which is a split of the sample that was used to generate BIR1.
[k] The accuracy of major element analyses by XRF is dominated by the precision [*Fitton et al.*, 1998].

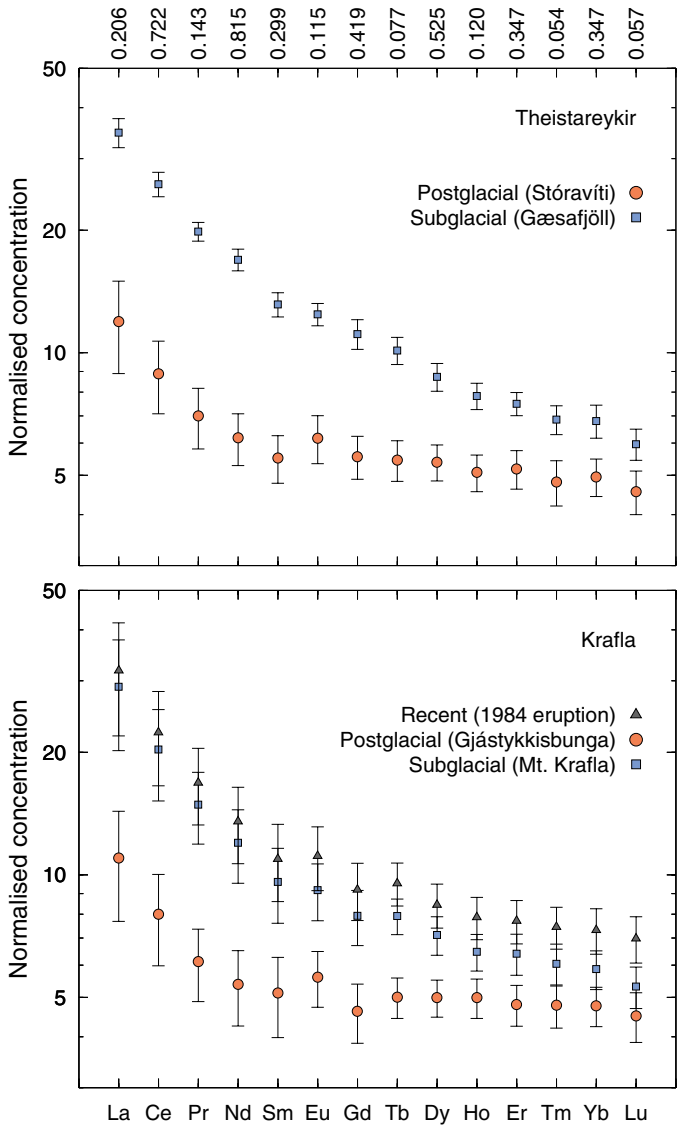

Figure 5. Concentrations of REEs in large eruptions from the Theistareykir and Krafla systems normalized to the MORB source of *McKenzie and O'Nions* [1991]. The normalizing value in ppm is shown for each REE at the top axis of Figure 5, top. The error bars show ±1 σ for the sample variability in each eruption.

the Lu content of Gæsafjöll is only a factor of 1.3 greater than that of Stóravíti.

[18] Large eruptions from the Krafla volcanic system show similar variations in REE content to those from the adjacent Theistareykir system. The largest postglacial eruption in Krafla is the lava shield Gjástykkisbunga which has a Mg # of 64.3 and very similar REE contents to Stóravíti (Figure 5). The Krafla table mountain, which is one of the largest preserved subglacial eruptions in the Krafla system, has a Mg # of 57.5 and REE contents that are higher than those of Gjástykkisbunga, and similar to those of Gæsafjöll. Therefore the change in composition between large glacial and early postglacial eruptions is not unique to Theistareykir and is repeated at Krafla. This repetition supports the argument that the changes in REE content are related to the glacial cycle.

[19] Krafla has been volcanically active in the last 1 kyr; the last eruptive episode took place between 1975 and 1984 [*Einarsson*, 1991]. Samples from the 1984 eruptive event have a mean Mg # of 54.0 and REE contents that are similar to large subglacial eruptions in the Krafla system (Figure 5). The

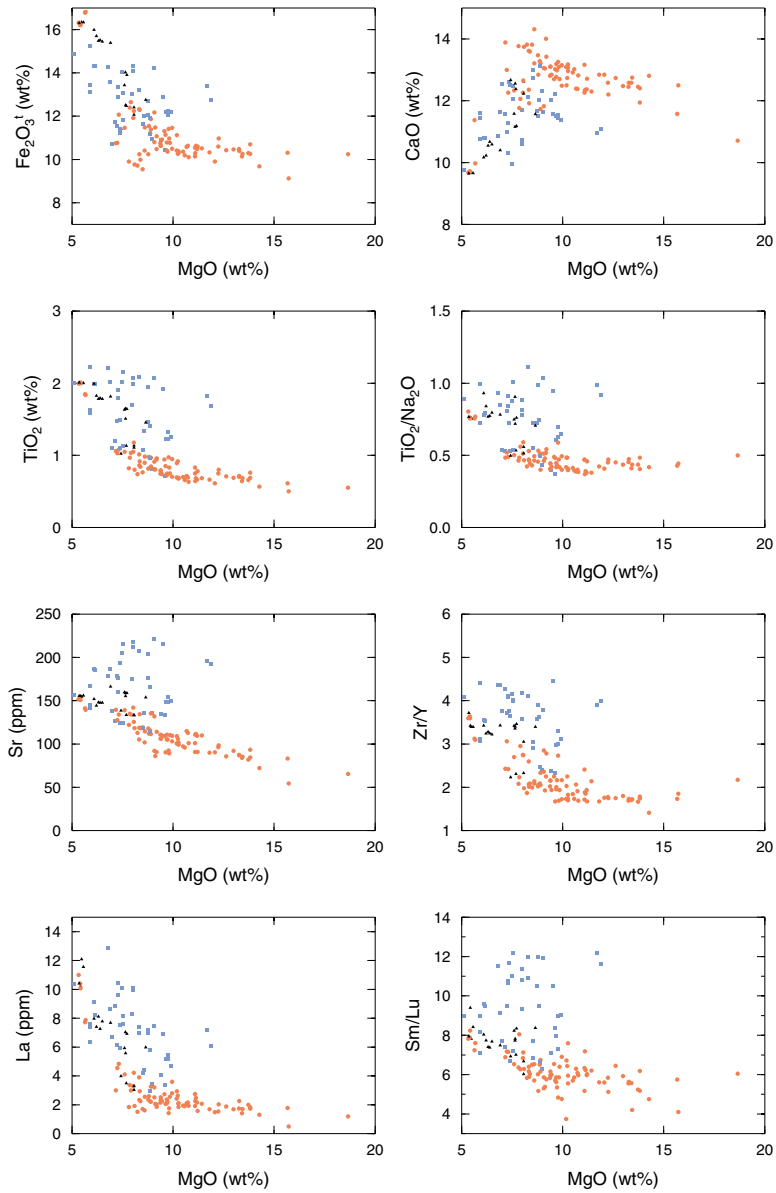

Figure 6. Concentrations and ratios of selected trace and major elements plotted against MgO for all Krafla and Theistareykir samples. Blue squares are glacial samples, orange circles are early postglacial samples (>7 kyr BP), and black triangles are recent samples (<7 kyr BP).

temporal evolution of REE compositions from the Krafla system is from high light REE contents during the glacial period, to low light REE contents during the early postglacial period and then a return to high light REE contents in later postglacial times.

4.3. Composition of All Samples

[20] The temporal variations in geochemistry in samples from Krafla and Theistareykir are not restricted to the large eruptions, nor to the REE concentrations of the samples. Figure 6 shows plots of major and trace element concentrations and ratios from the Krafla and Theistareykir samples against MgO content. Samples from glacial and later postglacial times have different compositions to those of early postglacial eruptions (12–7 kyr BP). At any given MgO content, the glacial eruptions have higher total FeO contents, lower CaO contents, and higher incompatible element concentrations. Although the largest eruptions from glacial and early postglacial times have similar MgO contents, the range of MgO contents observed in the early post-

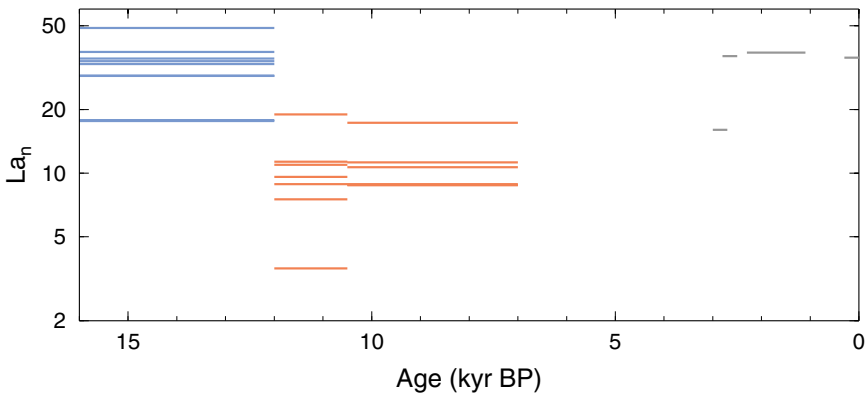

Figure 7. Temporal evolution of Krafla and Theistareykir eruption geochemistry. Each line shows the La concentration of an eruption, normalized to the MORB source of *McKenzie and O'Nions* [1991]. The length of the line shows the age bounds on the eruption. The glacial data are based on 53 samples from 9 eruptions, the early postglacial are based on 127 samples from 11 eruptions, and the recent are based on 16 samples from 6 eruptions.

glacial samples is greater than than of the glacial samples. While the highest MgO contents found in glacial samples are ~12 wt%, the most mafic picrites from Theistareykir contain over 20 wt% MgO. Some of the picrites contain up to 22 vol% accumulated olivine, so it is likely that the high MgO content of the picrites is caused in part by olivine accumulation (see Table 2 for modal analyses).

4.4. Timing of Variation

[21] The average La contents and age bounds of the largest mafic eruptions at Krafla and Theistareykir during the last 74 kyr are shown in Figure 7. Although it is not possible to give the subglacial eruptions absolute dates, the drop in volume-averaged REE concentrations after the end of the glacial period is likely to be real, since no subglacial eruptions with estimated volume greater than 0.3 km^3 have mean La concentrations under 5.5 ppm, while the early postglacial average is ~2 ppm. Ages of eruptions in the early postglacial period are poorly known due to the large gap between the bounding ash layers at 10.5 kyr BP and 7 kyr BP. The result of this uncertainty is that while the duration of the peak in eruption rates is well constrained (<1.5 kyr), the length of time that the REE concentrations of eruptions remains low is not well known (<8 kyr).

5. Modelling

[22] A number of models have been proposed to account for either the increase in eruption rates or the change in magma composition or both. Models of the increase in eruption rates are based on either increased tapping of magma chambers or an increase in melt production rate following deglaciation. *Gudmundsson* [1986] proposed a model where variation in the stress state of the crust during deglaciation and isostatic rebound produces an increase in eruption rate. In the model the crust is treated as a plate with an effective elastic thickness of ~400 m which overlies a magma reservoir. The model results show that if excess magma pressure in the reservoir reaches 32 MPa in response to deglaciation then the volume fraction of the reservoir that contributes to eruptions will be ~10 times higher in early postglacial times than in glacial times. In this model, the increase in eruption rates results from increased tapping of magma chambers following deglaciation. *Kelemen et al.* [1997] have also suggested that the peak in eruption rates after ice unloading could be caused by release of magma that was stored in crustal chambers during the glacial period.

[23] An alternative mechanism for increasing eruption rates was proposed *Jull and McKenzie* [1996], who argued that the pressure drop associated with removal of an ice sheet will increase melting rates since mantle under mid-ocean ridges melts by decompression. A simple calculation shows that this is a plausible argument. If the average Icelandic crustal thickness is produced by melting of mantle upwelling at the full spreading rate of 2 cm yr^{-1}, then the removal of a 2 km thick ice sheet in 1 kyr, equivalent to the removal of rock at 60 cm

yr^{-1}, will increase melt production rates by a factor of 30. *Jull and McKenzie* [1996] calculated the response of mantle with a Maxwell viscoelastic rheology to ice unloading in terms of a rate of depressurization as a function of time and position. Then, they used the melt fraction against depth relationship for mantle with a potential temperature of 1500°C to calculate the change in melt production rate caused by deglaciation. Their model results showed that during deglaciation the melt production rates were 30 times higher than during either glacial or later postglacial times.

[24] Models of the temporal variation in geochemistry also fall into two different categories. The variation in mantle melting rate as a function of depth predicted by the decompression models of *Jull and McKenzie* [1996] results in variation of the composition of mantle melts produced during the glacial cycle. They calculated that melts generated during deglaciation should have lower light REE concentrations than those generated during other times and therefore matched the sense of the change in observed REE concentrations.

[25] In a study of the Reykjanes Peninsula, *Gee et al.* [1998a] argued that the distinctive geochemistry of early postglacial lava compared to eruptions of other ages is due to shortened storage times in magma chambers caused by crustal instability during ice unloading and rebound. A key part of their argument is that crustal processes are capable of producing geochemical signatures that are typically interpreted as an indication of changing mantle melting conditions (e.g., changes in the Nb/Zr ratio). However, *Gee et al.* [1998a] did not quantify the magma chamber processes in terms of degree of fractionation/assimilation required.

[26] In the next few subsections the new observations from section 4 are used to assess the ability of mantle melting and magma chamber models to reproduce the temporal variation in magma composition observed at Krafla and Theistareykir.

5.1. Mantle Melting

[27] The model results of *Jull and McKenzie* [1996] predicted that during deglaciation the REE concentrations of the light REEs were ~15% less than those during steady-state melting (i.e., when there is no change in ice sheet size). However, the observed light REE concentration of subglacial eruptions is about a factor of 3 greater than that of early postglacial eruptions. The change in geochemistry between subglacial and early postglacial magma predicted by the model is controlled by both the melt fraction against depth relationship and the change in decompression rate caused by unloading. The models of *Jull and McKenzie* [1996] give low REE concentrations for lava produced during deglaciation because the greatest increase in melting rate takes place at 60 km depth, where the mantle has been depleted by ~15% melting. *Slater et al.* [1998] developed an inversion model where the melt fraction against depth relationship was allowed to vary until the best fit to the relative changes in REE concentrations between Gæsafjöll and Stóravíti was obtained. The inversion model produces an excellent fit to the relative changes in REE concentrations between the two eruptions (Figure 8). The best fit melt fraction against depth model is similar to that expected for mantle with a potential temperature of 1500°C but has a low melt fraction tail that extends to greater depths than the 1500°C model. The crustal thickness calculated from this melt function using the method of *White et al.* [1992] is 20.1 km, similar to the thickness of ~20.5 km found in a seismic study at Krafla [*Staples et al.*, 1997]. The melting model was also used to predict the compositional variation for selected incompatible trace elements, and the Zr, Y, Sr, and Ti concentrations calculated for melts from glacial times are a factor of 1.5–2.5 times higher than those for early postglacial melts. These predicted increases are of a similar magnitude to those observed at Theistareykir. The relative changes in REE contents between the large eruptions from the Krafla system, shown in Figure 5 can also be matched using the inversion models of *Slater et al.* [1998].

[28] The variation in average melt composition between glacial and early postglacial times predicted by the models of *Jull and McKenzie* [1996] and *Slater et al.* [1998] reflects a variation in the relative weighting of instantaneous fractional melt

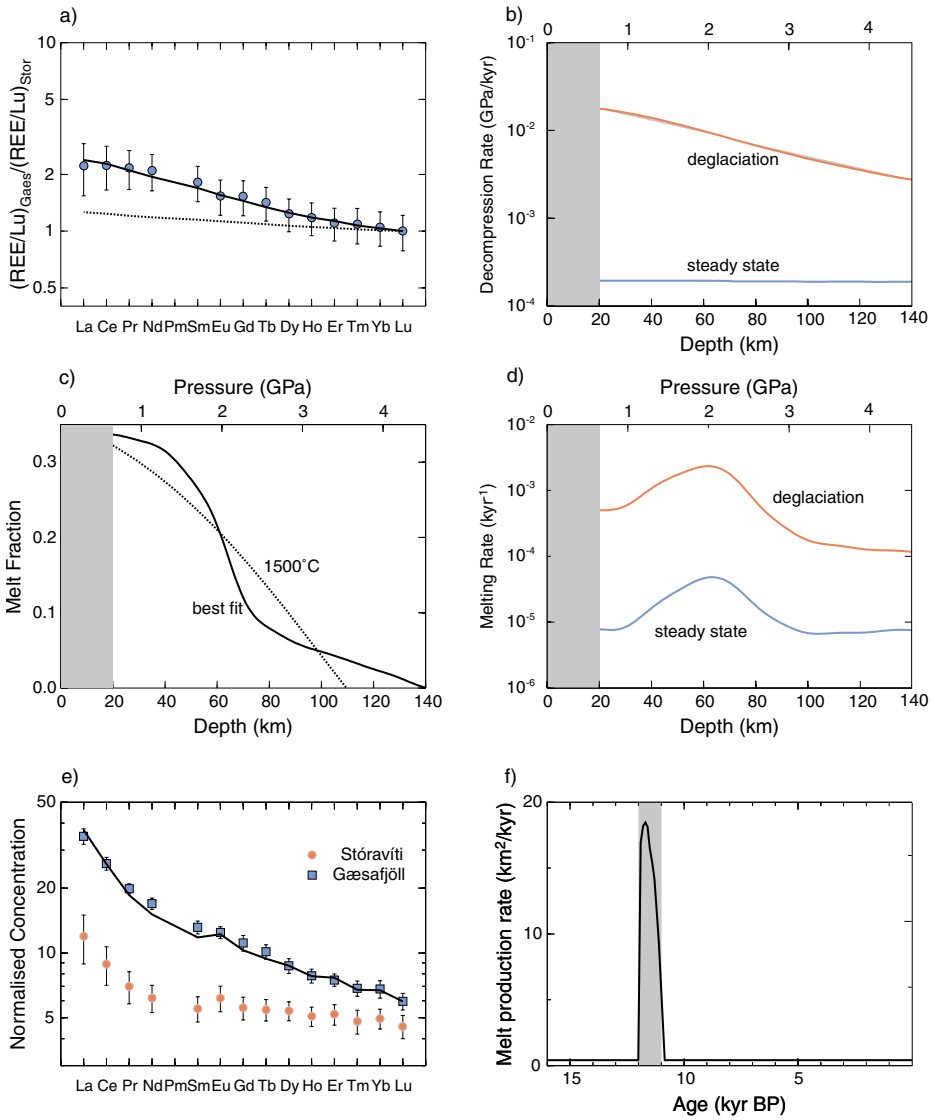

Figure 8. (a) REE concentrations of Gæsafjöll and Stóravíti normalized using the method of *Slater et al.* [1998]. The solid line is the result of the best fit inversion model. The dotted line is the result of the initial melt model, which is the melt fraction against depth for mantle with a potential temperature of 500°C predicted from the parameterization of *Watson and McKenzie* [1991]. (b) Horizontal average of decompression rates in the melting region during steady state (no change in ice-sheet dimensions) and deglaciation. The deglaciation decompression rates are the average from the unloading period. The grey area represents the crust. (c) Best fitting melt fraction against depth curve. Also shown in a dashed line is the predicted melting curve for mantle with a potential temperature of 1500°C. Garnet is stable at depths >80 km and spinel is stable at depths <100 km. (d) Horizontal average of melt production rate. (e) REE concentrations of Gæsafjöll and Stóravíti normalized to depleted mantle source of *McKenzie and O'Nions* [1991]. Line is model fit to Gæsafjöll from Figure 8a, multiplied by the REE/Lu ratios for Stóravíti and then the Lu concentration of Gæsafjöll. (f) Total melt production rate through time. The grey shaded area is the time of ice unloading in the model.

compositions from different parts of the melting region. The weighting used in the models is calculated from the decompression history that results from the glacial unloading. The total range of instantaneous melt compositions that can be produced during fractional melting is much larger than the predicted shift from average glacial to average early postglacial compositions. Part of this compo-

sitional range will be present in the Theistareykir and Krafla lavas if the deglaciation history is different to that used in the model or if the fractional melts are not well mixed before eruption. The method of *White et al.* [1992] was used to calculate instantaneous fractional melt compositions for the best-fit melt fraction against depth relationship shown in Figure 8. The calculated range of incompatible element concentrations in the instantaneous fractional melts is much larger than the observed range and, for example, the predicted La concentration varies from 0–43 ppm, Sr from 0–1361 ppm, Sm/Lu from 0–75.3, and Zr/Y from 0–10.61.

[29] The melting models of *Jull and McKenzie* [1996] are not suitable for calculating the compositional variation of elements that do not have simply defined partition coefficients and therefore these models cannot reproduce the variation in FeO and CaO between glacial and early postglacial eruptions. Nonetheless it is well known that FeO and CaO contents can be influenced by the depth and extent of melting. Peridotite melts produced at high pressures have higher FeO contents than low pressure melts and the CaO content of the melt increases with degree of melting until the point of clinopyroxene exhaustion from the residue [*Langmuir et al.*, 1992; *Hirschmann et al.*, 1999]. Therefore the relatively low FeO and high CaO contents of early postglacial eruptions may result from increased melting of shallow mantle as predicted by the models of *Jull and McKenzie* [1996].

[30] It is not yet clear whether the MgO content of the mantle melts produced during early postglacial times is different to that of the glacial times. While the MgO contents of early postglacial whole-rock samples range to much higher values than those of glacial times, much of this variation may be due to olivine accumulation. For example, the Theistareykir picrite samples, which have 15.7–21.5 wt % MgO, contain 12–22 vol% olivine crystals. These olivine crystals are highly forsteritic and have 45–50 wt % MgO [*Maclennan et al.*, 2001a]. If the picrite whole-rock compositions are corrected for olivine accumulation, then a range in estimated melt compositions of 10–17 wt% MgO is obtained, with an average of 12.3 wt% MgO. These estimates are likely to be in error for samples which have a heterogeneous distribution of olivine, where the thin section may not be representative of the portion of the sample used for major element analyses. *Maclennan et al.* [2001a] proposed that Theistareykir mantle melts had MgO contents between 13 and 16 wt% because a number of samples in this compositional range contained <2 vol% accumulated olivine and because the composition of these samples is in Mg-Fe equilibrium with mantle olivines (Fo_{90-92}). If the most magnesian glacial samples, from Gæsafjöll, have their compositions corrected for modest olivine accumulation then the estimated melt composition has 11.2 wt% MgO. However, these samples may have undergone fractional crystallization prior to eruption.

5.2. Magma Chamber Processes

[31] Crystallization within magma chambers and assimilation of crustal material from their walls will alter the composition of magma as it passes through the crust before eruption. The temporal variation in the composition of magma from the Reykjanes Peninsula has been attributed to a shorter residence time of melt in the crust during early postglacial times [*Gee et al.*, 1998a]. These workers argue that lavas from early postglacial times have compositions that are similar to those of unmodified mantle melts and that the average composition of the mantle melts is not required to vary with time. Therefore, in the modelling of magma chamber processes that is presented below, the composition used as the initial melt is that of an early postglacial sample from the Borgarhraun flow that has high MgO contents and low La contents.

5.2.1. Crystallization and Accumulation

[32] As described in section 5.1, the range in MgO contents of early postglacial samples is greater than that of eruptions from other times and some early postglacial picrites have up to 20 wt% MgO. These high MgO samples come from small-volume eruptions that contain accumulated olivine. Eruptions with large amounts of accumulated olivine (>10 vol %) appear to be restricted to early postglacial times. It is likely that the eruption of flows with large amounts of accumulated oli-

vine results from changes in magma chamber behavior during and shortly after deglaciation, rather than directly from variations in mantle melting. Inspection of Figure 6 shows that simple fractional crystallization or accumulation is not likely to the be the sole cause of the difference in composition between the glacial/recent and early postglacial eruptions. Olivine, plagioclase, and clinopyroxene are the most abundant phases present in the Krafla and Theistareykir samples and fractional crystallization of these phases can account for almost all of the variation in the major element contents of those samples [*Maclennan et al.*, 2001a]. However, fractional crystallization of these phases cannot produce the large variation observed in incompatible element concentrations (e.g., La, Sr) and ratios (Sm/Lu, TiO_2/Na_2O) at fixed MgO content.

[33] Similarly, it is not likely that the variation of incompatible trace element ratios such as Nb/Zr in lava from the Reykjanes peninsula results from fractional crystallization. *Gee et al.* [1998a] suggested that such variation may be caused by more complex crystallization models such as replenished-tapped-fractionated (RTF) magma chambers [*O'Hara and Mathews*, 1981] or in situ crystallization [*Langmuir*, 1989]. Equation (15) of *O'Hara and Mathews* [1981] and equation 6 of *Langmuir* [1989] were used to calculate the compositional range that can be generated by the RTF and in situ processes respectively. The in situ crystallization models produced a wider range of compositions than the RTF models, so in Figure 9 only the results of the in situ models are shown. Of the phases found within the Krafla and Theistareykir samples, clinopyroxene has the most important control on the REE behavior during crystallization. However, the variation in Sm and Lu concentrations and Sm/Lu ratio between early postglacial and glacial eruptions cannot be reproduced by in situ models with clinopyroxene as the sole crystallizing phase or by gabbro crystallization. The reason for this is that there is not a great enough difference in the partition coefficients of Sm and Lu in clinopyroxene to produce the observed Sm and Lu variation. However, garnet has very different Sm and Lu partition coefficients and in situ crystallization of garnet-bearing material may be able to account for the variation in Sm and Lu contents (Figure 9c). However, garnet has never been found as a phenocryst or xenocryst in samples from this area, and it is not required to describe major element fractionation paths. For garnet to crystallize from primitive basaltic magma pressures of >1.5 GPa are required [*Bernstein*, 1994], equivalent to depths of 45 km, greater than the crustal thickness at Krafla (20 km) and the maximum depth of crystallization for primitive Theistareykir magmas (30 km) estimated by *Maclennan et al.* [2001a]. Therefore the circumstances under which crystallization models can produce the observed variation in incompatible element contents at Krafla and Theistareykir are at odds with petrological and geological observations from the area.

5.2.2. Crustal Assimilation

[34] Assimilation of crustal materials from the margins of magma chambers may influence the trace element geochemistry of the erupted lava. Studies of basalts from the Theistareykir system [*Eiler et al.*, 2000] and the Reykjanes peninsula [*Gee et al.*, 1998b] suggest that crustal assimilation produces variation in basalt composition, and *Gee et al.* [1998a] proposed that the temporal variations in basalt composition may result in part from lower degrees of crustal assimilation during early postglacial times. If assimilation of crustal material is the cause of the high incompatible element concentrations of glacial/later postglacial basalt compared to those of early postglacial basalts then the assimilant must also have higher Sm/Lu and TiO_2/Na_2O ratios than those of the early postglacial primitive basalts (Figure 6). Assimilation of basalt from Krafla or Theistareykir is not likely to be the cause of the variation in incompatible element concentrations of the basalts themselves. Rhyolite lava found at Krafla and Theistareykir has high REE contents and is thought to be generated during partial melting of hydrothermally altered crust in the margins of shallow magma chambers [*Jónasson*, 1994]. However, the rhyolite magma is not an appropriate assimilant because it has Sm/Lu ratios that lie within the range of the analysed basalts (Sm/Lu $\sim$ 11) and lower TiO_2/Na_2O ratios than any of the basalts (TiO_2/

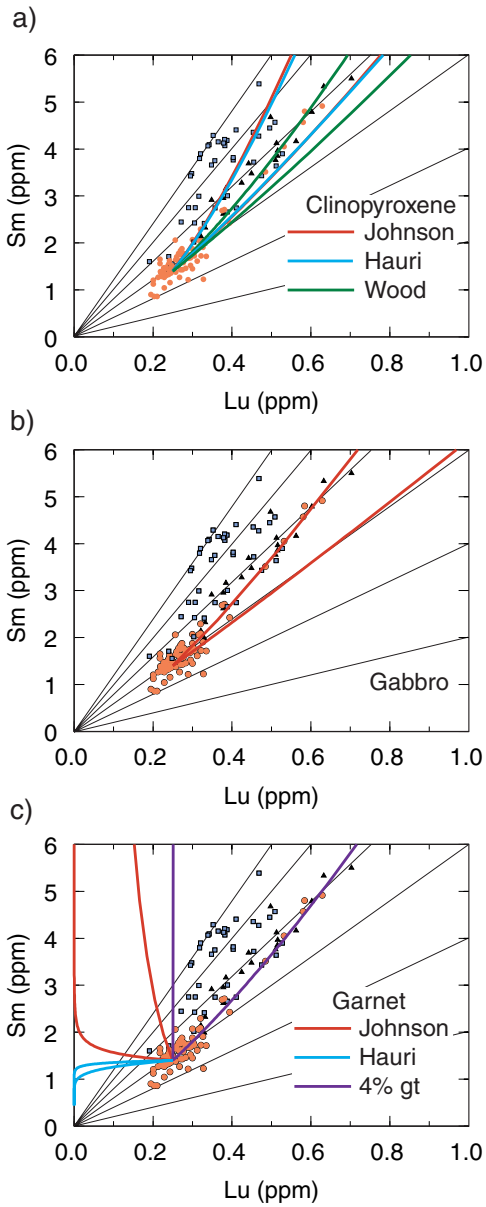

$Na_2O \sim 0.1$). The geochemical trends of postglacial basalts from Theistareykir have been attributed to partial assimilation of an andesitic material by *Eiler et al.* [2000]. However, the andesite composition proposed by these workers has high REE contents but a low TiO_2/Na_2O ratio of ~0.5, and assimilation of this melt cannot produce the compositional variation between glacial and early postglacial lava.

[35] Limited amounts of crustal melting may produce melts with high REE concentrations, and at small melt fractions, the melt will have a Sm/Lu ratio that is a factor D_{Lu}/D_{Sm} times higher than that of the solid. Therefore melting in the presence of garnet can produce magma with Sm/Lu up to 30 times higher than those of the original material, while melting in the presence of clinopyroxene can only increase the ratio by a factor of 1.5. Melting of basalt or gabbro with similar composition to the average Theistareykir lava composition will be able to produce melts with high Sm/Lu as long as sufficient garnet is present during melting. Variable assimilation of this material into primitive Theis-

Figure 9. (opposite) Results of in situ crystallization modelling. Sample symbols are the same as Figure 6. The thin lines show constant Sm/Lu from 2 to 14. The thick colored lines show the extremes of the model results, and only compositions between these lines can be generated by each crystallizing assemblage. (a) Crystallization of clinopyroxene alone. Red lines show results for the partition coefficients from *Johnson* [1998], where $D_{Sm}^{cpx} = 0.293$, $D_{Lu}^{cpx} = 0.449$, and light blue lines are those from *Hauri et al.* [1994] with $D_{Sm}^{cpx} = 0.462$, $D_{Lu}^{cpx} = 0.623$. The green line was produced with partition coefficients calculated using the method of *Wood and Blundy* [1997], and the clinopyroxene compositions are the average of those from Theistareykir [*Maclennan et al.*, 2001a]. The calculated coefficients at 1250°C and 1.5 GPa were $D_{Sm}^{cpx} = 0.592$ and $D_{Lu}^{cpx} = 0.656$. (b) Effect of crystallization of a gabbro with 10% olivine, 40% clinopyroxene, and 50% plagioclase. The partition coefficients for clinopyroxene were those of *Johnson* [1998] and the values of *McKenzie and O'Nions* [1991] were used for olivine and plagioclase. (c) Effect of garnet crystallization. Red curves calculated with the partition coefficients of *Johnson* [1998], where $D_{Sm}^{gt} = 0.25$ and $D_{Lu}^{gt} = 7.1$, blue curves were calculated using the coefficients of *Hauri et al.* [1994] with $D_{Sm}^{gt} = 1.1$ and $D_{Lu}^{gt} = 3.79$ and purple curves were calculated for a material containing 4% garnet with the *Johnson* [1998] coefficients and 96% minerals with $D_{Sm}^{gt} = D_{Lu}^{gt} = 0$.

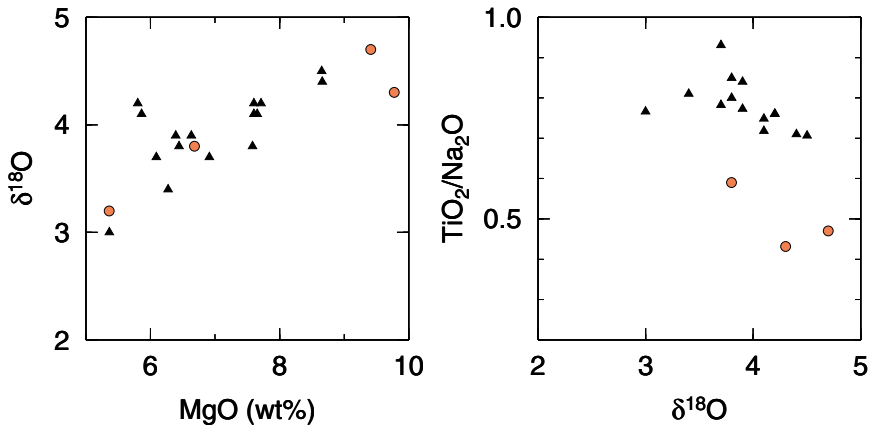

Figure 10. Oxygen isotope, MgO, and TiO_2/Na_2O compositions of Krafla samples [*Nicholson et al.*, 1991].

tareykir melts can then reproduce the observed variation in Sm/Lu ratio in the Theistareykir basalts. However, *Springer and Seck* [1997] found that garnet is only stable above 1.0 GPa during experimental melting of metabasalts and metagabbros. This pressure corresponds to a depth greater than the bottom of the crust under Krafla and Theistareykir [*Staples et al.*, 1997]. Small degrees of melting of a gabbro with 50% plagioclase will produce melts with Sr content similar to that of the gabbro because $D_{Sr}^{plg} \sim 2$ and $D_{Sr}^{cpx} \sim D_{Sr}^{ol} \sim 0$. The Sr content of Gæsafjöll is 1.8 times higher than that of Stóravíti and melting of material with a bulk composition similar to that of Stóravíti cannot produce this variation unless the material contains <25% plagioclase. The metagabbroic and metabasaltic compositions reported by *Springer and Seck* [1997] only contain <40% plagioclase at pressures greater than 1.0 GPa.

[36] Further evidence that crustal assimilation does not play an important role in the generation of the temporal variation in geochemistry of the rift zone basalts comes from oxygen isotope measurements. Assimilation of hydrothermally altered material will decrease the $\delta^{18}O$ of the melt from mantle values of ~5 per mil toward that of Icelandic meteoric water, about −10 per mil [*Nicholson et al.*, 1991; *Eiler et al.*, 2000]. While the Theistareykir data of *Eiler et al.* [2000] is exclusively from the early postglacial period, *Nicholson et al.* [1991] analyzed $\delta^{18}O$ in both early postglacial and young flows (<3 kyr BP). At a given $\delta^{18}O$ value, young basalts have higher TiO_2/Na_2O than early postglacial samples (Figure 10). It is not likely that the increase in TiO_2/Na_2O results from assimilation of hydrothermally altered crustal materials. Geochemical observations from the Reykjanes peninsula also show that the temporal variation in incompatible element ratios does not always correlate with indicators of residence time in the crust. For example, the geochemistry of the Stapafell subglacial eruption [*Gee et al.*, 1998b], whose age falls outside the time period studied by *Gee et al.* [1998a], indicates that it has undergone little fractional crystallisation (13.9 wt% MgO) or crustal assimilation ($\delta^{18}O_{ol} \sim 5.0$ per mil). Nonetheless, Stapafell has some of the highest Nb/Zr values of the samples reported by *Gee et al.* [1998b]. Early postglacial eruptions with high MgO contents and $\delta^{18}O_{ol}$ have the lowest Nb/Zr. This observation is consistent with models which predict temporal variation in the composition of magma supplied to the crust.

5.3. Mantle Source Variations

[37] The rate of melt production and the geochemistry of melt generated during mantle melting are controlled by the temperature and composition of the mantle in the melting region. Therefore, changing the nature of mantle entering the melting region will alter melt production. The matter of interest here is whether changing the material supplied to the melting region can produce large variation in total melt production rate and average melt composition on timescales of a few thousand years. If changes in the composition of mantle entering the melting

region control the temporal variation in eruption rates and lava composition at Krafla, Theistareykir, and on the Reykjanes Peninsula then the association between these changes and deglaciation is coincidental. There is no clear reason why mantle entering the melting region at the time of deglaciation should be different to that entering at other times.

[38] A simple calculation shows that a thermal anomaly in the mantle supplied to the melting region cannot produce a sharp burst in melt production that lasts under 1000 years. The characteristic time of decay of such an anomaly, during which the magnitude of the anomaly is reduced by a factor of e, is given by the $t_c = a^2/\pi^2\ \kappa$ where κ is the thermal diffusivity and a is the relevant length scale. This standard expression is derived from a one-dimensional diffusion equation. In 1 kyr, mantle upwelling at the Icelandic half spreading rate of 1 cm yr^{-1} will travel 10 m. If we set a at 10 m and κ at 8×10^{-7} m^2 s^{-1}, then the characteristic time is less than 1 year. Since the timescale of mantle convection is several million years, such spatially restricted thermal anomalies cannot exist in the mantle entering the melting region under Iceland.

[39] The diffusion time of chemical anomalies in solid mantle is $\sim 10^{10}$ times longer than that of thermal anomalies and this sluggish diffusion allows small geochemical heterogeneities to be preserved in the mantle. *Hirschmann and Stolper* [1996] proposed that garnet pyroxenite might be widespread in the mantle and that it could be important during basalt petrogenesis since it starts to melt ~15 km deeper than standard mantle peridotite and has a high melt productivity near its solidus. If mantle with a high proportion of garnet pyroxenite had entered the melting region for 1 kyr at the time of deglaciation, then melt production rates would have been increased. The magnitude of the increase in melt production rates is dependent on the vertical distance over which the more fusible mantle moves because this distance controls the amount of decompression melting.

[40] The average cross-sectional melt production rate at Theistareykir, the product of the crustal thickness and the full spreading rate, is 400 m^2 yr^{-1}. If mantle is upwelling in a corner flow with a wedge angle of 45° [see *Jull and McKenzie*, 1996] then the average upwelling rate of mantle will be the half spreading rate, u. Therefore, in ~1 kyr a vertical thickness, T_g, of 10 m of mantle will enter the melting region. If garnet pyroxenite starts to melt at 150 km depth under Iceland then the width of the melting region, W_g at this depth will be 300 km. The cross-sectional melt production rate from the garnet pyroxenite is then $W_g T_g u (DX/Dz)_g$, where $(DX/Dz)_g$ is the productivity of garnet pyroxenite near its solidus. *Hirschmann and Stolper* [1996] have estimated that this initial productivity is close to 0.6% km^{-1}. The estimated cross sectional melt production rate from the garnet pyroxenite is therefore 0.018 m^2 yr^{-1}, only a fraction of a percent of the average cross-sectional melt production rate at Krafla. Therefore it seems unlikely that the 30–50 fold increase in eruption rates during early postglacial times was caused by the introduction of mantle of a different composition to the melting region.

[41] The magnitude and timescale of temporal variation in lava composition that results from changes in the composition of mantle entering the melting region is also controlled by the melt productivity. After deglaciation, the La contents of the Theistareykir and Krafla eruptions double over a period of less than ~5 kyr, and the temporal variations in composition observed by *Gee et al.* [1998a] at the Reykjanes peninsula take place over a period of less than 2 kyr. The impact of the introduction of new material to the melting region on the composition of the average melt produced is controlled by the melt generation rate. If garnet pyroxenite enters the melting region for 5 kyr then the cross-sectional melt production from the garnet pyroxenite will be 0.9 m^2 yr^{-1}, a factor of 400 less than the average melt production rate. Therefore if addition of the melts of the garnet pyroxenite is to double the average La content of the average mantle melt, the La concentration in the garnet pyroxenite melts must be a factor of 450 greater than those of the initial average melt or ~1000 ppm.

6. Discussion

[42] It is likely that the effect of glacial unloading on both mantle melting and magma chambers

processes influences the temporal variation in geochemistry observed at Krafla, Theistareykir, and the Reykjanes Peninsula. The observed changes in incompatible element concentrations and ratios can be produced by variation in the rate of mantle melting. However, the presence of high MgO lava (>15 wt%) is restricted to early postglacial eruptions from Theistareykir and this shift in the range of observed MgO contents may reflect a change in the behavior of magma chambers during the early postglacial period, as suggested by *Gee et al.* [1998a]. Therefore it is also likely that the high eruption rates of early postglacial times result both from increased mantle melting rates and from enhanced tapping of magma chambers. Although the relative importance of these two processes is not yet clear, the relative timing of the unloading event and the burst in eruption rates can be used to constrain melt velocities within the crust and mantle. Eruption rates are unusually high for <2 kyr after deglaciation and the geochemical anomaly lasts for 2–9 kyr at Theistareykir and Krafla and 4 kyr on the Reykjanes Peninsula [*Gee et al.*, 1998a]. The similar duration of the period of high eruption rates and that of low incompatible element contents of the eruptions indicates that the increased eruption rates reflect increased supply of melt to the crust. If the high eruption rates result from increased mantle melting rates then the vertical velocity of melt in the mantle can be estimated as outlined below.

[43] Finite melt extraction velocities were incorporated into the melt generation models to investigate how the melt supply rate from the mantle to the surface changes as extraction rate is varied. The melt generation rates were calculated as a function of time using the decompression rates from the ice unloading models and the melt fraction against depth curve of *Slater et al.* [1998] shown in Figure 8. The greater the depth that melt is generated at, the longer it will take to reach the surface. The time at which a packet of mantle melt reaches the surface was calculated as $t_s = t_g + z_g/v_z$ where t_g is the time of melt generation, z_g is the depth where the melt packet is generated and v_z is the vertical melt velocity. The melt supply rate was then calculated as a function of time t by summing all the melt packets with $t = t_s$. The results

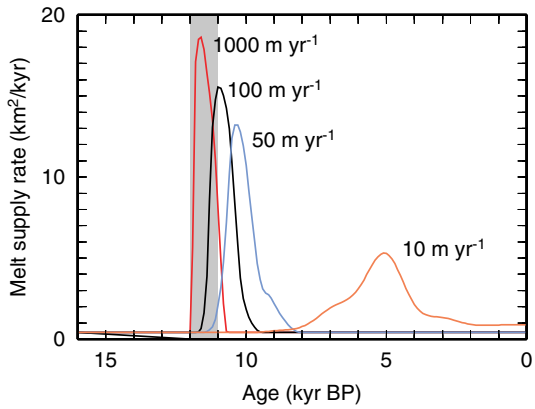

Figure 11. Predicted melt supply rates from the mantle to the crust when finite melt extraction velocities are incorporated into the melt generation model shown in Figure 8. The light grey box shows the period of ice unloading in the model.

of this integration are shown for a range of melt velocities in Figure 11.

[44] When melt extraction velocities are 50 m yr^{-1} or lower, the predicted length of the burst is over 2 kyr and finishes more than 2 kyr after the end of ice unloading, which does not match the observations. If the model is run with melt extraction velocities of 100 m yr^{-1} or more, the results are consistent with the observations. The predicted supply rate of melt from the mantle to the crust depends on the melt fraction against depth relationship used, and if melting is restricted to shallow levels, lower minimum extraction velocities will account for the observations. However, the minimum extraction velocity required to match the observations is still 50 m yr^{-1} when melting starts ~70 km depth; in models that fit the geochemistry and crustal thickness of northern Iceland [*Nicholson and Latin*, 1992; *Slater et al.*, 1998], melting starts at over 70 km. A velocity of 50 m yr^{-1} or more is consistent with observations of uranium series disequilibrium in basalts from ocean islands and mid-ocean ridges [*Richardson and McKenzie*, 1994]. Since simple porous flow cannot produce extraction velocities over 2 m yr^{-1} in the mantle [*Kelemen et al.*, 1997], it is likely that melt is transported by porous channels or fractures [*Richardson et al.*, 1996; *Kelemen et al.*, 1997]. Channelized flow has also been proposed on the basis of the shape

and geochemistry of dunite bodies in the mantle section of several ophiolite complexes [*Kelemen et al.*, 1997].

7. Conclusions

[45] Eruption rate histories for four parts of the Icelandic rift zones were estimated using published maps and bounds on the ages of eruptions. Eruption rates immediately after deglaciation were 30–50 times higher than those from more recent times. These high eruption rates persisted for <1.5 kyr after the deglaciation of each area.

[46] New compositional data presented for 80 basalt and picrite samples from the Krafla and Theistareykir volcanic systems shows that there is a temporal variation in both the major and trace element composition of lava from the Krafla and Theistareykir volcanic systems in NE Iceland. At a given MgO content, eruptions from glacial times have higher incompatible element concentrations than those from early postglacial times. Early postglacial lavas show a greater spread in MgO contents than those from glacial times, with some early postglacial eruptions having >15 wt% MgO. Eruptions from the last 3 kyr at Krafla have similar compositions to those from glacial times. These temporal variations in composition are present for both large and small eruptions from Krafla and Theistareykir.

[47] The high eruption rates and low REE concentrations in the lava from early postglacial times can be accounted for by increased melt generation rates in the shallow mantle caused by unloading of an ice sheet.

[48] Models of processes that alter magma composition in magma chambers, such as fractional crystallization and crustal assimilation, cannot produce the observed change in REE geochemistry between subglacial and early postglacial eruptions unless garnet is an important phase in magma chamber processes. However, there is no evidence of the presence of garnet in magma chambers under northern Iceland.

[49] Changing the composition of mantle entering the melting region at the time of deglaciation has little effect on melt generation rates, so is unlikely to be the cause of the postglacial burst in volcanism or the geochemical variation.

[50] If the peak in eruptive activity is primarily caused by increased mantle melting rates and mantle melting is accelerated by ice unloading, the temporal relationship between deglaciation and the burst in eruption rates is controlled by melt extraction velocity. Since the burst finished less than 2 kyr after deglaciation, melt extraction velocities of more than 50 m yr^{-1} are required. Such velocities cannot be produced by simple porous flow and require melt flow to be in channels or fractures in the mantle.

Appendix A. Analytical Techniques

[51] The techniques used by *Nicholson* [1990], *Slater* [1996], and *Maclennan* [2000] to obtain the data shown in Table 2 are outlined below.

A.1. X-Ray Fluorescence Analysis

[52] The powdered samples were prepared for X-ray fluorescence (XRF) analysis at the University of Edinburgh, using the technique described by *Fitton et al.* [1998]. Fusion discs for major and minor element analysis were made after mixing sample powder with lithium tetraborate flux. This flux acts to absorb heavy elements during analysis. The samples were dried for at least 4 hours in an oven at 110°C, and then a nominal but precisely weighed 1 g of sample was ignited at 1100°C. Then the samples were mixed with the flux, fused, poured, and cast into discs as described by *Fitton et al.* [1998]. Trace element concentrations were determined on pressed powder samples which contained 6 g of sample and four drops of a 2% aqueous solution of polyvinyl alcohol. The discs were run on a Philips PW 1480 automatic X-ray fluorescence spectrometer with a Rh-anode X-ray tube and the analytical conditions are given by *Fitton et al.* [1998]. The spectrometer was calibrated with USGS and CRPG standards using the values given by *Jochum et al.* [1990] for Nb and Zr and *Govindaraju* [1994] for the other elements.

A.2. Inductively Coupled Plasma Mass Spectrometry

[53] The samples were prepared for ICP-MS analysis by HF dissolution at the University of Cambridge. The powders were dried overnight and 0.5000 ± 0.0003 g of powder were weighed into clean teflon beakers. A few drops of millipore water were added to make a slurry and then 6 mL of Aristar conc. HF and 10 mL Aristar conc. HNO_3 were poured into the beaker. The beakers were covered and the samples refluxed for 4 hours after which time the powder had been digested. Then the sample solutions were left to evaporate to near dryness (this takes between 1 and 2 hours) and a sludge was left at the base of the beaker. Then 5 mL Aristar conc. HNO_3 was added to the residue and the samples were refluxed for 2 hours under lids and then evaporated to near dryness. A further 5 mL HNO_3 was added, and the solutions were refluxed for 2 hours. These solutions were then transferred to 250 mL volumetric flasks and the flasks were filled to 250 mL with millipore water. At this stage the samples were at 1:500 dilution. The flasks were then left to stand overnight on a hot plate and the solutions were transferred to 60 mL nalgene bottles which were sealed. Procedural blank solutions were prepared along with each batch of samples and each reference standard was prepared with more than one batch.

[54] The sample solutions were analyzed for REEs (and also Ga and Co in one sesssion by Slater) on the research machine at the NERC ICP-MS facility, Centre for Analytical Research in the Environment at Silwood Park, Ascot. The sample solutions were diluted by another factor of 10 to 1:5000 to reduce suppression. For REE analysis only the mass range from ^{139}La to ^{172}Lu was scanned and calibration solutions at low concentrations were used with solutions at 2, 5, and 10 ppb. Throughout the analyses the lowest concentration calibration solution was run as a drift monitor every five samples. The procedural blanks were under 1% of the lowest sample concentrations measured, and all the measurements were over 200 times the detection limits. The ICP-MS machine was washed with dilute nitric acid between each sample run. Analyses of reference materials were interspersed with the unknowns. The repeat measurements given in Table 2 are based on repeat runs of standard solutions over the two days that it took to analyze each sample set. These estimates also reflect any noise introduced during the preparation procedure because the solutions for the reference materials were prepared several times.

Acknowledgments

[55] The authors would like to thank NERC and the Royal Society for support. Godfrey Fitton and Hugh Nicholson kindly provided the Krafla samples and data. The assistance of Paul Mason and the staff of the NERC ICP-MS facility at Silwood Park is acknowledged. Nick Arndt and Godfrey Fitton are thanked for their reviews and Catherine Chauvel and Bill White for reviews and editorial advice. This is Department of Earth Sciences contribution ES7022.

References

Andrews, J. T., J. Hardardóttir, G. Helgadóttir, A. E. Jennings, A. Geirsdoóttir, A. E. Sneinbjörnsdóttir, S. Schoolfield, G. B. Kristjánasdóttir, L. M. Smith, K. Thors, and J. P. M. Syvitski, The N and W Iceland Shelf: Insights into Last Glacial Maximum ice extent and deglaciation based on acoustic stratigraphy and basal radiocarbon AMS dates, *Quat. Sci. Rev.*, *19*, 619–631, 2000.

Bernstein, S., High-pressure fractionation in rift-related basaltic magmatism: Faeroe plateau basalts, *Geology*, *22*, 815–818, 1994.

Björck, S., Ó. Ingólfsson, H. Haflidason, M. Hallsdóttir, and N. J. Anderson, Lake Torfadalsvatn: A high resolution record of the North Atlantic ash zone 1 and the last glacial-interglacial environmental changes in Iceland, *Boreas*, *21*, 15–22, 1992.

Eiler, J. M., K. Grönvold, and N. Kitchen, Oxygen isotope evidence for the origin of chemical variation in the lavas of Theistareykir volcano in Iceland's Northern Volcanic Zone, *Earth Planet. Sci. Lett.*, *184*, 269–286, 2000.

Einarsson, P., Umbrotin vid Kröflu, in *Náttúra Mývatns*, edited by A. Gardarsson and A. Einarsson, pp. 97–139, Hid islenska náttúrufrædifélg, Reykjavik, 1991.

Einarsson, P., and K. Sæmundsson, Map accompanying the festschrift *Í HLUTARINS EDLI*, Menningarsjódur, Reykjavik, 1987.

Elliott, T. R., C. J. Hawkesworth, and K. Grönvold, Dynamic melting of the Iceland plume, *Nature*, *351*, 201–206, 1991.

Fitton, J. G., A .D. Saunders, L. M. Larsen, B. S. Hardarson, and M. J. Norry, Volcanic rocks from the southeast Greenland margin at 63°N: Composition, petrogenesis and mantle sources, *Proc. Ocean Drill. Program Sci. Results*, *152*, 331–350, 1998.

Gee, M. A. M., R. N. Taylor, M. F. Thirlwall, and B. J. Mur-

ton, Glacioisostacy controls chemical and isotopic characteristics of tholeiites from the Reykjanes Peninsula, SW Iceland, *Earth Planet. Sci. Lett.*, *164*, 1–5, 1998a.

Gee, M. A. M., M. F. Thirlwall, R. N. Taylor, D. Lowry, and B. J. Murton, Crustal processes: Major controls on Reykjanes Peninsula lava chemistry, SW Iceland, *J. Petrol.*, *39*, 819–839, 1998b.

Geirsdóttir, A., J. Hardardóttir, and A. E. Sveinbjörnsdóttir, Glacial extent and catastrophic meltwater events during the deglaciation of Southern Iceland, *Quat. Sci. Rev.*, *19*, 1749–1761, 2000.

Govindaraju, K., 1994 compilation of working values and sample description for 383 geostandards, *Geostand. Newsl.*, *18*, 1–158, 1994.

Grönvold, K., N. Óskarsson, S. J. Johnsen, H. B. Clausen, C. U. Hammer, G. Bond, and E. Bard, Ash layers from Iceland in the Greenland GRIP ice core correlated with oceanic and land sediments, *Earth Planet. Sci. Lett.*, *135*, 149–155, 1995.

Gudmundsson, A., Mechanical aspects of postglacial volcanism and tectonics of the Reykjanes Peninsula, Southwest Iceland, *J. Geophys. Res.*, *91*, 12,711–12,721, 1986.

Hardarson, B. S., and J. G. Fitton, Increased mantle melting beneath Snaefellsjökull volcano during late Pleistocene deglaciation, *Nature*, *353*, 62–64, 1991.

Hauri, E. H., T. P. Wagner, and T. L. Grove, Experimental and natural partitioning of Th, U, Pb and other trace-elements between garnet, clinopyroxene and basaltic melts, *Chem. Geol.*, *117*, 149–166, 1994.

Hirschmann, M. M., and E. M. Stolper, A possible role for garnet pyroxenite in the origin of the garnet signature in MORB, *Contrib. Mineral. Petrol.*, *124*, 185–208, 1996.

Hirschmann, M. M., M. S. Ghiorso, and E. M. Stolper, Calculation of peridotite partial melting from thermodynamic models of minerals and melts, II, Isobaric variations in melts near the solidus and owing to variable source composition, *J. Petrol.*, *40*, 297–313, 1999.

Ingólfsson, Ó., and H. Norddahl, A review of the environmental history of Iceland, 13,000–9,000 yr BP, *J. Quat. Sci.*, *9*, 147–150, 1994.

Ingólfsson, Ó., H. Norddahl, and H. Haflidason, Rapid isostatic rebound in southwestern Iceland at the end of the last glaciation, *Boreas*, *24*, 245–259, 1995.

Ingólfsson, Ó., S. Björck, H. Haflidason, and M. Rundgren, Glacial and climatic events in Iceland reflecting regional north Atlantic climatic shifts during the Pleistocene-Holocene transition, *Quat. Sci. Rev.*, *16*, 1135–1144, 1997.

Ito, G., Y. Shen, G. Hirth, and C. J. Wolfe, Mantle flow, melting and dehydration of the Iceland mantle plume, *Earth Planet. Sci. Lett.*, *165*, 81–96, 1999.

Jakobsson, S. P., J. Jónsson, and F. Shido, Petrology of the western Reykjanes Peninsula, Iceland, *J. Petrol.*, *19*, 669–705, 1978.

Jennings, A. E., J. Syvitski, L. Gerson, K. Grönvold, A. Geirsdóttir, J. Hardardóttir, J. Andrews, and S. Hagen, Chronology and paleoenvironments during the late Weichselian deglaciation of the southwest Iceland shelf, *Boreas*, *29*, 167–183, 2000.

Jochum, K. P., H. M. Seufert, and M. F. Thirlwall, High sensitivity Nb analysis by spark-source mass spectrometry (SSMS) and calibration of XRF Nb and Zr, *Chem. Geol.*, *81*, 1–16, 1990.

Johnson, K. T. M., Experimental determination of partition coefficients for rare earth and high-field-strength elements between clinopyroxene, garnet, and basaltic melt at high pressures, *Contrib. Mineral. Petrol.*, *133*, 60–68, 1998.

Jónasson, K., Rhyolite volcanism in the Krafla central volcano, north-east Iceland, *Bull. Volcanol.*, *56*, 516–528, 1994.

Jull, M., and D. McKenzie, The effect of deglaciation on mantle melting beneath Iceland, *J. Geophys. Res.*, *101*, 21,815–21,828, 1996.

Kelemen, P. B., G. Hirth, N. Shimizu, M. Spiegelman, and H. J. B. Dick, A review of melt migration processes in the adiabatically upwelling mantle beneath oceanic spreading ridges, *Philos. Trans. R. Soc. London Ser. A*, *355*, 283–318, 1997.

Langmuir, C. H., Geochemical consequences of in situ crystallisation, *Nature*, *340*, 199–205, 1989.

Langmuir, C. H., E. M. Klein, and T. Plank, Petrological systematics of mid-ocean ridge basalts: Constraints on melt generation beneath ocean ridges, in *Mantle Flow and Melt Generation at Mid-ocean Ridges*. *Geophys. Monogr. Ser.*, vol. 71, edited by J. Phipps Morgan et al., pp. 183–280, AGU, Washington, D.C., 1992.

McKenzie, D., and R. K. O'Nions, Partial melt distributions from inversion of rare earth element concentrations, *J. Petrol.*, *32*, 1021–1091, 1991.

Maclennan, J., Melt generation and movement under Northern Iceland, Ph.D. Thesis, Univ. of Cambridge, Cambridge, U.K., 2000.

Maclennan, J., D. McKenzie, K. Grönvold, and L. Slater, Crustal accretion under northern Iceland, *Earth Planet. Sci. Lett.*, *191*, 295–310, 2001a.

Maclennan, J., D. McKenzie, and K. Grönvold, Plume-driven upwelling under central Iceland, *Earth Planet. Sci. Lett.*, *194*, 67–82, 2001b.

Mayewski, P., and M. Bender, The GISP2 ice core record – Palaeo climate highlights, *U.S. Natl. Rep. Int. Union Geod. Geophys. 1991–1994*, *Rev. Geophys.*, *33*, 1287–1296, 1995.

Nicholson, H., The magmatic evolution of Krafla, NE Iceland, Ph.D. Thesis, Univ. of Edinburgh, Edinburgh, U.K., 1990.

Nicholson, H., M. Condomines, J. G. Fitton, A. E. Fallick, K. Grönvold, and G. Rogers, Geochemical and Isotopic Evidence for Crustal Assimilation Beneath Krafla, Iceland, *J. Petrol.*, *32*, 1005–1020, 1991.

Nicholson, H., and D. Latin, Olivine tholeiites from Krafla, Iceland: Evidence for variations in melt fraction within a plume, *J. Petrol.*, *33*, 1105–1124, 1992.

O'Hara, M. J., and R. E. Mathews, Geochemical evolution in an advancing, periodically replenished, periodically tapped, continuously fractionated magma chamber, *J. Geol. Soc. London*, *138*, 237–277, 1981.

Richardson, C., and D. McKenzie, Radioactive disequilibria from 2D models of melt generation by plumes and ridges, *Earth Planet. Sci. Lett.*, *128*, 425–437, 1994.

Richardson, C. N., J. R. Lister, and D. McKenzie, Melt con-

duits in a viscous porous matrix, *J. Geophys. Res.*, *101*, 20,423–20,432, 1996.

Rossi, M. J., Morphology and mechanism of eruption of postglacial shield volcanoes in Iceland, *Bull. Volcanol.*, *57*, 530–540, 1996.

Rundgren, M., Biostratigraphic evidence of the Allerod-Younger Dryas-Preboreal oscillation in Northern Iceland, *Quat. Res.*, *44*, 405–416, 1995.

Rundgren, M., Ó. Ingólfsson, S. Björck, H. Jiang, and H. Haflidason, Dynamic sea level change during the last deglaciation of northern Iceland, *Boreas*, *26*, 201–215, 1997.

Sæmundsson, K., Outline of the geology of Iceland, *Jökull*, *29*, 7–28, 1980.

Sæmundsson, K., Jardfrædi Kröflukerfisins, in *Náttúra Mývatns*, edited by A. Gardarsson and A. Einarsson, pp. 24–95, Hid islenska náttúrufrædifélg, Reykjavik, 1991.

Sæmundsson, K., Geology of the Thingvallavatn area, *Oikos*, *64*, 40–68, 1992.

Sæmundsson, K., *Svartsengi, geological map (bedrock)*, 1:25,000, Orkustofnun, Hitaveita Sudurnesja and Landmælingar Íslands, Reykjavik, Iceland, 1995.

Sigmundsson, F., and P. Einarsson, Glacio-isostatic crustal movements caused by historical volume change of the Vatnjökull ice cap, Iceland, *Geophys. Res. Lett.*, *19*, 2123–2126, 1992.

Sigvaldason, G. E., K. Annertz, and M. Nilsson, Effect of glacier loading/deloading on volcanism: Postglacial volcanic production rate of the Dyngjufjöll area, central Iceland, *Bull. Volcanol.*, *54*, 385–392, 1992.

Slater, L., Melt generation beneath Iceland, Ph.D. Thesis, Univ. of Cambridge, Cambridge, U.K., 1996.

Slater, L., M. Jull, D. McKenzie, and K. Grönvold, Deglaciation effects on mantle melting under Iceland: Results from the northern volcanic zone, *Earth Planet. Sci. Lett.*, *164*, 151–164, 1998.

Slater, L., D. McKenzie, K. Grönvold, and N. Shimizu, Melt generation and movement under Theistareykir, NE Iceland, *J. Petrol.*, *42*, 321–354, 2001.

Springer, W., and H. A. Seck, Partial fusion of basic granulites at 5 to 15 kbar: implications for the origin of TTG magmas, *Contrib. Mineral. Petrol.*, *127*, 30–45, 1997.

Staples, R. K., R. S. White, B. Brandsdóttir, W. Menke, P. K. H. Maguire, and J. H. McBride, Färoe-Iceland Ridge Experiment, 1, Crustal structure of northeastern Iceland, *J. Geophys. Res.*, *102*, 7849–7866, 1997.

Stuiver, M., and P. J. Reimer, Extended ^{14}C data base and revised ^{14}C calibration program, *Radiocarbon*, *35*, 215–230, 1993.

Vilmundardóttir, E., and G. Larsen, Productivity pattern of the Veidivötn fissure swarm, Southern Iceland, in postglacial times. Preliminary results: paper presented at 17e Nordiska Geologmötet, Helsingsfors Univ., Helsinki, Finland, 1986.

Watson, S., and D. McKenzie, Melt generation by plumes: A study of Hawaiian volcanism, *J. Petrol.*, *32*, 501–537, 1991.

White, R. S., D. McKenzie, and R. K. O'Nions, Oceanic crustal thickness from seismic measurements and rare earth element inversions, *J. Geophys. Res.*, *97*, 19,683–19,715, 1992.

Wood, B. J., and J. D. Blundy, A predictive model for rare earth element partitioning between clinopyroxene and anhydrous silicate melt, *Contrib. Mineral. Petrol.*, *129*, 166–181, 1997.